Faculdade de Engenharia da Universidade do Porto

Development of Multifunctional Solid Lipid Nanoparticles for Theranostic Applications in Rheumatoid Arthritis

João Pedro Albuquerque e Costa

bio09013@fe.up.pt

Dissertation for the Master Thesis in Bioengineering

Major in Biomedical Engineering

Supervisor: Bruno Sarmento

Co-Supervisor: Salette Reis

June 2014

- This Page was intentionally left blank -

© João Albuquerque, 2014

Summary

This work was submitted as a Master Thesis in partial fulfillment of the requirements for the degree of Master of Science in Bioengineering at the Faculty of Engineering, University of Porto. It was conducted under the guidance of Professor Bruno Filipe Carmelino Cardoso Sarmento, PhD, Affiliated Researcher at INEB – Instituto de Engenharia Biomédica and Assistant Professor at Instituto Superior de Ciências da Saúde-Norte (ISCS-N), CESPU, and under the co-supervision of Professor Maria de La Salette de Freitas Fernandes Hipólito Reis Dias Rodrigues, Associate Professor at Faculty of Pharmacy, University of Porto and Affiliated Researcher at GABAI – REQUIMTE.

The research experimental work was performed in the Faculty of Pharmacy, University of Porto, at the department of Chemical Sciences – Applied Chemistry in collaboration with INEB and ISCS-N.

Thesis defense took place at the Faculty of Engineering, University of Porto, on the 15th of July, 2014. The Master Thesis was evaluated with a final score of 18 out 20 possible points.

- This Page was intentionally left blank -

Abstract

Rheumatoid Arthritis (RA) is the most common autoimmune disease related to the joints and one of the most severe. Despite the intensive investigation, RA inflammatory process remains unknown and finding effective and long lasting therapies that specifically target RA is a challenging task. In RA the pro-inflammatory macrophages persist in the inflammation site and frequently overexpress cytokines and other biomolecule factors that amplify even more the inflammatory process. However, during RA, the macrophages also overexpress the CD64 surface marker that drives the search for new specific RA therapies.

This work proposed an innovative approach for RA therapy, taking advantage of the new emerging field of nanomedicine and the tools that it offers for targeted therapies. This study aimed to develop a targeted theranostic system for intravenous administration, using Solid Lipid Nanoparticles (SLN), a biocompatible and biodegradable colloidal delivery system, widely researched for medical applications, to function as a drug delivery system. The SLNs were encapsulated with methotrexate (MTX) and superparamagnetic iron oxide nanoparticles (SPIONs), to be used as therapeutic and imaging agents, respectively. The SLNs were also surface-functionalized with an anti-CD64 antibody that specifically targets RA-infected macrophages.

A total of eight different cetyl palmitate and stearic acid SLN formulations were produced using in an organic solvent-free emulsification-sonication method that combined high shear homogenization and ultra-sonication in order to compare the influence of each component present (MTX, SPIONs and anti-CD64) on NP characteristics. Particle size was assess by dynamic light scattering and analyzed by transmission electron microscopy and surface charge (zeta potential) mas measured by phase analysis light scattering. The placebo formulations showed sizes around 160 nm and zeta potentials of – 40 mV. Results also showed that MTX did not influence significantly NP properties, whereas SPIONs encapsulation caused an increase in both size and zeta values. The antibody conjugation caused an increased in zeta potential as expected but an unexpected decrease in NP size was observed. However, all the formulations presented sizes below 200 nm and zeta values lower than -12 mV, indicating suitable characteristics as nanosystems for intravenous administration. The stability of these formulations was also proven up to one month for the non-conjugated formulations. Nanoparticle morphology was analyzed by transmission electron microscopy (TEM).

TEM photographs indicated that the SPIONs were encapsulated inside the SLN matrix. Also, it was possible to observe small deformity and aggregation of NPs, while formulations without SPIONs presented a spherical shape with little aggregation. FT-IR was used to confirm the presence of MTX in the SLNs as well as the successful conjugation of the antibody to the SLN.

MTX association efficiency was determined by UV/Vis spectrophotometry, rendering values non-lower than 98% for both MTX-loaded SLNs and MTX- and SPIONs-loaded SLNs.

In vitro studies were performed with THP-1 cells and enabled to assess the cytotoxicity of the developed formulations. MTT and LDH assays demonstrated that the formulations were biocompatible and presented low cytotoxicity a concentrations lower than 500 μg/mL, but there were no significant changes when comparing the different formulations at the same concentrations unexpectedly.

This study could provide an effective and viable approach for future theranostic strategies. It was proven that the proposed NP were not cytotoxic, that both a therapeutic and imaging agent could be co-encapsulated and the SLN functionalized for a potential future application such as anti-body specific targeting.. The proposed formulations are, therefore, promising candidates for future theranostic applications.

"A single dream is more powerful than a thousand realities"

J. R. R. Tolkien

- This Page was intentionally left blank -

Acknowledgements

I would like to express my gratitude to both Professor Bruno Sarmento and Professor Salette Reis, for giving me the opportunity to work with their respective research groups and for their availability, support and guidance during the thesis research and experimental work. And also to all the members of both the already mentioned research groups for their assistant and welcoming attitude.

I would also like to thank Catarina Moura, for all of her assistance, prompt availability, support and, above all, patience over these last few months.

I would also like to acknowledge Engineering and Metal&Bio, for all the moments and lessons that they have provided, and I hope that they will continue to provide, over the last five years of my life. In particular to all the wonderful people that begun their studies in the Faculty of Engineering in the year 2009 and to my three precious goddaughters, Tweety, Teló and Mourinho, as well as the newest member of the family, Leppy, my granddaughter for always being there whenever I need, not matter the reason or time.

I would also like to thank, from the bottom of my heart, my family but specially my parents for always, always being there of basically making me the man I am today. To Leonor for all of her love and patience, for always being there over the last two years of my life.

Last I also like to thank a man who is no longer among, but that it had a great influence in getting me here, to my high school Math teacher José Carlos Carvalho, may his soul rest in peace.

- This Page was intentionally left blank -

Table of Contents

List of Figures

List of tables

- This Page was intentionally left blank -

Glossary

List of Abbreviations

ACPA	Anti-Citrullinated Peptides Antibody
AU	Arbitrary Units
BBB	Brain-Blood-Barrier
BSA	Bovine Serum Albumin
CMC	Critical Micelar Concentration
DLS	Dynamic Light Scattering
DMARD	Disease-Modifying Anti-Rheumatic Drug
DMEM	Dulbecco's Modified Eagle's Medium
DMSO	Dimethyl Sulfoxide
EDC	1-Ethyl-3-(3-dimethylaminopropyl) Carbodiimide Hydrochloride
FEUP	*Faculdade de Engenharia da Universidade do Porto*
FFUP	*Faculdade de Farmácia da Universidade do Porto*
FLS	Fibroblast-Like Synoviocytes
FT-IR	Fourier Transform InfraRed
GABAI	*Grupo de Análises Bioquímicas Ambientais e Industriais*
HPH	High Pressure Homogenization
HPLC	High Performance Liquid Chromatography
Ig	Immunoglobulin
IL	Interleukin
INEB	*Instituto Nacional de Engenharia Biomédica*
ISCS-N	*Instituto Superior de Ciências da Saúde – Norte*
LDH	Lactate Dehydrogenase
mAb	Monoclonal Antibody
MES	2-Morpholinoethanesulfonic Acid
MLS	Macrophage-Like Synoviocytes

MMP	Matrix MetalloProteinase
MRI	Magnetic Resonance Imaging
MTT	3-(4,5-Dimethylthiazol-2-yl)-2,5-diphenyltetrazolium bromide
MTX	Methotrexate
NHS	N-Hydroxysulfosuccinimide
NLC	Nanostructured Lipid Carrier
NP	Nanoparticle
NSAID	Non-Steroidal Anti-Inflammatory Drug
PALS	Phase Analysis Light Scattering
PBS	Phosphate Buffer Saline
PdI	Polydispersity Index
PEG	Polyethylene Glycol
RA	Rheumatoid Arthritis
REQUIMTE	*Rede de Química e Tecnologia*
SEM	Scanning Electron Microscopy
SLN	Solid Lipid Nanoparticle
SPION	Superparamagnetic Iron Oxide Nanoparticle
TEM	Transmission Electron Microscopy
TNF-α	Tumor Necrosis Factor – alfa

1. Introduction

1.1. The Joint

Muscles pull on bone to make them move, but movement would be impossible without joints. Joints allow the skeleton to be flexible, enabling it to bend in certain locations that in turn allows movement at different degrees around those locations while, simultaneously, providing protection for the same [1]. A joint, or articulation, is an anatomical location where two or more bones come together and can be classified into three groups depending on the type of structures that binds these bones: fibrous, cartilaginous and synovial [1, 2].

In a fibrous joint bones are united by a fibrous, collagen rich, connective tissue and have no joint cavity. This type of joint can be found between the bones of the skull, for instance. Cartilaginous joints are similar to fibrous joints but, in their turn, they are connected by cartilage, being it hyaline or fibrocartilage. An example of a cartilaginous joint is the manubriumsternal joint (between the manubrium and sternum). Synovial joints are more complex than fibrous and cartilaginous joints. In a synovial joint bones are not directly joined, the articular extremities of the bone are encapsulated in a synovial cavity by dense connective tissue and often strengthened by complementary ligaments as shown in Figure 1-1. An example of a synovial joint is the acromioclavicular joint (between the acromium and the clavicle) [1, 2].

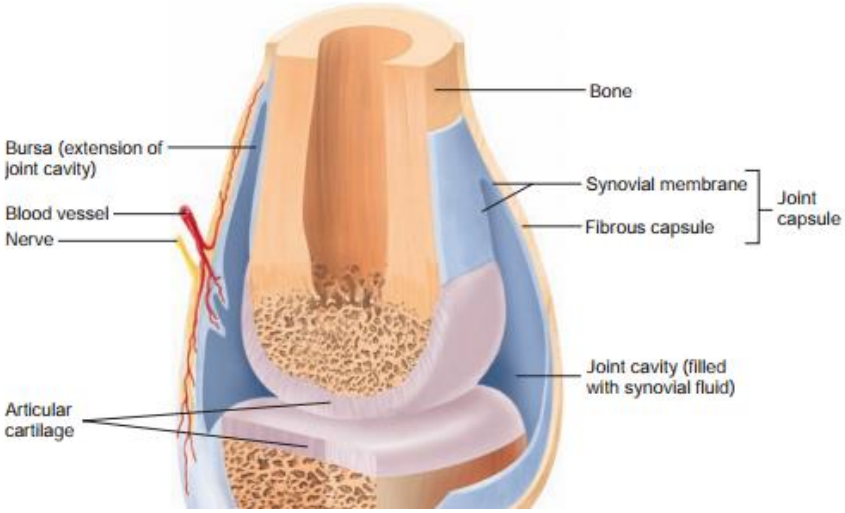

Figure 1-1 – Structure of a synovial joint. Adapted from [1].

The different constituents of a synovial joint are described in detail below:

1. Joint capsule – composed by an outer fibrous capsule that may be attached to auxiliary ligaments, and an inner synovial membrane, also known as *synovium*, that secretes the

synovial fluid and contains two cell types, macrophage-like synoviocytes (MLS) and fibroblast-like synoviocytes (FLS). The joint capsule stabilizes and provides protection to the articulation;

2. Joint cavity – space comprised by the joint capsule and filled with synovial liquid. This liquid, containing hyaluronic acid and lubricin, provides lubrication, shock absorption and nourishment to the joint and bones;
3. Articular cartilage – hyaline cartilage covers the bone inside the synovial cavity increasing shock absorption and reducing friction between bones during movements [1-3].

Joints can also be classified according to the type and degree of movement allowed: i) synarthrosis, when they allow little to no mobility, ii) amphiarthrosis, when they allow slight mobility, and iii) diarthrosis, when they allow free mobility. This functional characterization is associated with their structural classification, thus most synarthrosis joints are fibrous joints, most amphiarthrosis joints are cartilaginous joints and all diarthrosis are synovial joints [1, 2].

1.2. Rheumatoid Arthritis

1.2.1. The Disease

Rheumatoid arthritis (RA) is a chronic systemic inflammatory disease of uncertain cause that affects 1% of the population of the developed world, being more common among women than men. RA usually develops in the fourth and fifth decade of life, with 80% of the total cases occurring between the ages of 35 and 50 [4-7]. It is also theorized that some individuals are more genetically susceptible to contract this disease than others [6, 8]. RA is often induced by an external agent (like cigarette smoking, infection or trauma) that triggers an autoimmune reaction, leading to synovial hypertrophy and chronic joint inflammation along with potential for extra-articular manifestations [4-8].

RA is usually a clinical syndrome spanning several disease subsets, which all lead towards a final common pathway in which persistent inflammation and associated damage to articular cartilage and underlying bone are present (figure 1-2). The primary symptoms of RA are pain, stiffness and swelling of the joints resulting in impaired physical function and movement. These symptoms are often accompanied by inherent symptoms such as fever and malaise. Although there are several associated mechanisms that trigger RA inflammation, the exact pathway that leads to it was not yet been determined [4-8].

The primary inflammation of RA starts in the synovium. An external factor induces the overproduction of TNF-α by MLS and FLS. In response, the tissue of the synovial lining enters hyperplasia, as a result of MLS and FLS proliferation and accumulation. This increased number of synoviocytes leads to an even higher production of TNF-α and an overproduction of many pro-inflammatory cytokines such as interleukin-6 (IL-6) and interleukin-1 (IL-1) that drive and maintain

the persistent inflammation and induce joint destruction, by increasing the production of matrix metalloproteinases (MMPs) and activating osteoclasts [4, 6, 7, 9]. It has also been observed that, in RA, FLS show abnormal behavior and may spread to other joints, supporting hypothesis that RA starts in joints [6].

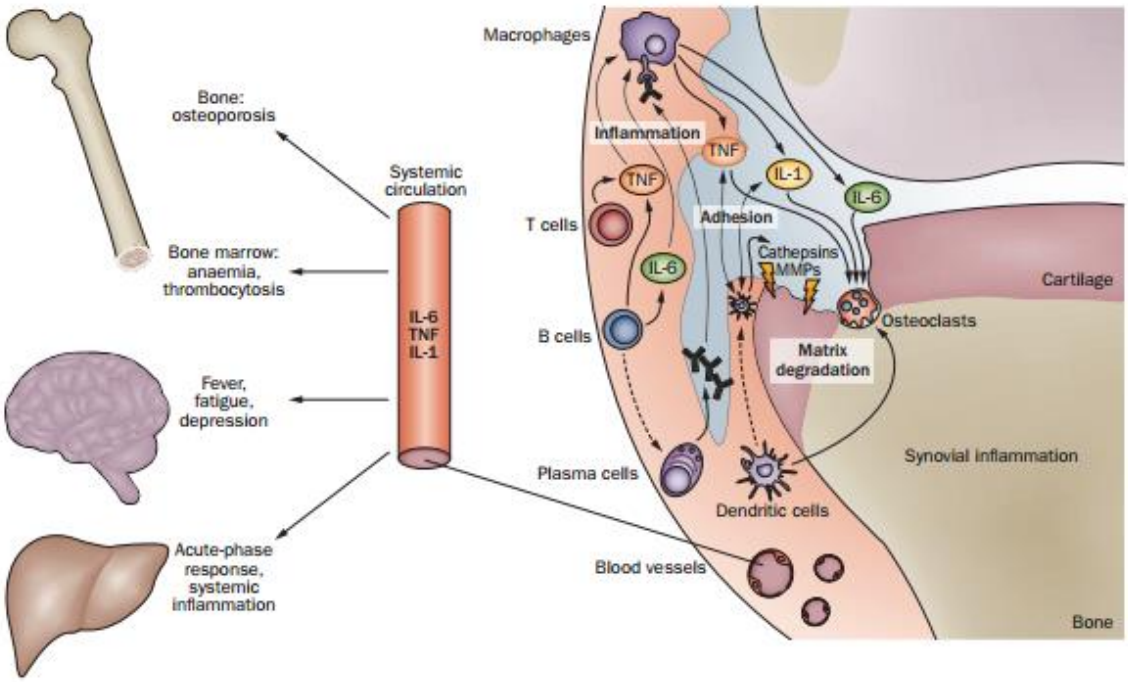

Figure 1-2 – Pathogenesis of RA: synovial and systemic inflammation. Adapted from [7].

Autoantibodies also play an important role in RA by wrongly targeting the body's own molecules as foreign or pathogenic. The main autoantibodies usually found in RA are rheumatoid factors (primarily IgM and IgA rheumatoid factors) and antibodies directed against citrullinated peptides (ACPA) located in the outer cellular membrane. In fact, 50-80% of all patients present at least one of these antibodies [6, 8]. It has also been registered that the presence of ACPA leads to histologically different types of RA, patients with ACPA (ACPA-positive) tend to have more lymphocytes in the synovial tissue; on the other hand, patients without ACPA (ACPA-negative) have increased fibrosis. Additionally, ACPA-positive RA is associated with increased joint damage and low remission rates [6].

1.2.2. Diagnosis, Management and Treatment

Early diagnosis and treatment have been recognized as essential for improving clinical outcomes in patients with rheumatoid arthritis. RA diagnosis is usually achieved by bloods tests or imaging techniques such as X-rays or magnetic resonance imaging (MRI) [4-6, 10]. However, diagnosis is somewhat difficult in the early stages of the disease since diagnostic criteria were developed from data obtained in patients with established rheumatoid arthritis, and therefore, are not readily applicable [11, 12].

In particular, MRI as demonstrated a greater sensitivity to early RA signs when compared to clinical examination or traditional radiology imaging. MRI allows for a direct visualization of the joint and enables the identification and analysis of the earliest histological and physiological alterations, making it a promising tool for an early RA diagnosis [5, 10-12].

Currently, there is no cure for RA, but some treatments are able to improve symptoms and hinder disease progression. These therapies aim to minimize symptoms such as articular pain and swelling, prevent bone erosion and deformity, and maintain joint functionality for daily activity. The best results with these treatments are obtained when they are initiated early and aggressively [4-6, 11, 13, 14].

Disease management is achieved primarily by using two main classes of medication: i) analgesics and non-steroidal anti-inflammatory drugs (NSAIDs) that lessen joint pain and stiffness, and disease-modifying anti-rheumatic drugs (DMARDs) that reduce joint swelling and pain, decrease acute-phase markers, limit progressive joint damage and improve function, by facilitating movement [5-7, 9, 13, 14].

The dominant DMARD in RA management is methotrexate (MTX), due to its proven efficacy, safety profile and low cost. MTX is an analogue of folic acid that ultimately disrupts cellular folate metabolism by inhibiting its target enzyme, the di-hydrofolate reductase. This drug seems to exert its anti-inflammatory effects by acting at different levels of the pathophysiological signaling cascade, directly inhibiting proliferation, pro-inflammatory cytokine production and inducing apoptosis in cells involved in immune and inflammatory reaction. These combined effects explain the overall anti-inflammatory action of MTX in the sustained management of RA [5, 6, 9].

New therapies are also been studied that consider the use of biological agents that target TNF-α and kinase receptors, in an attempt to disrupt RA signaling pathways, as well as the use of glucocorticoids to diminish synovial inflammation [6, 7, 13-16]. Despite recent developments and intensive research in RA, there is no definitive cure for the disease. Additionally, most of these treatments are also not targeted, leading to drug accumulation in undesired locations that may cause complications [6, 7, 13, 14].

1.3. Nanomedicine

Nanotechnology is the understanding and manipulation of materials whose dimensions range between 1-100 nm and has been in the forefront of much research in the past decades. Although nanotechnology comprises dimensions between 1-100 nm other systems consider materials with more than 100 nm to be applications of nanotechnology [17]. Traditionally, nanoparticles (NPs) are made of metals, ceramics and inorganic semiconductors. However, NPs can also be made of organic polymers, colloids or biomolecules, including DNA, proteins and lipids. This alternative approach is known as soft nanotechnology. This research led to innumerous applications, in particular the

application of this technology to medicine gave rise to nanomedicine [18-23]. As a consequence of the intensive work done in the area of nanotechnology, biocompatible colloidal systems, such as matrix NPs, micellar systems and conjugates have been developed. These systems enable nanomedicine applications for drug delivery and tissue regeneration strategies [17, 20, 22, 24].

Nanomedicine allowed the development of many drug delivery systems. Due to the side-effects of many drugs, nanoparticulate drug delivery systems were designed in order to achieve fewer complications. The main objective of using colloidal drug delivery systems is the reduction of systemic side-effects and maintenance of appropriate drug concentration in the required place. In these systems NPs are more interesting when compared with microparticles, since they possess a greater cell uptake, which is desirable when the drug is intended to penetrate the cellular membrane [20, 22, 24, 25].

The possibility of NP multi-functionalization opens the path for a novel and widespread medical applications based on nanomedicine strategies. (Figure 1-3). NPs have the potential to carry therapeutic and/or imaging agents, for theranostic applications. They can be conjugated to a specific ligand, such as antibodies, to target a specific tissue or organ or facilitate cellular penetration. They can also be used to avoid/bypass bio-barriers and macrophage uptake, by coating the NP with polyethylene glycol (PEG), for example [26-36].

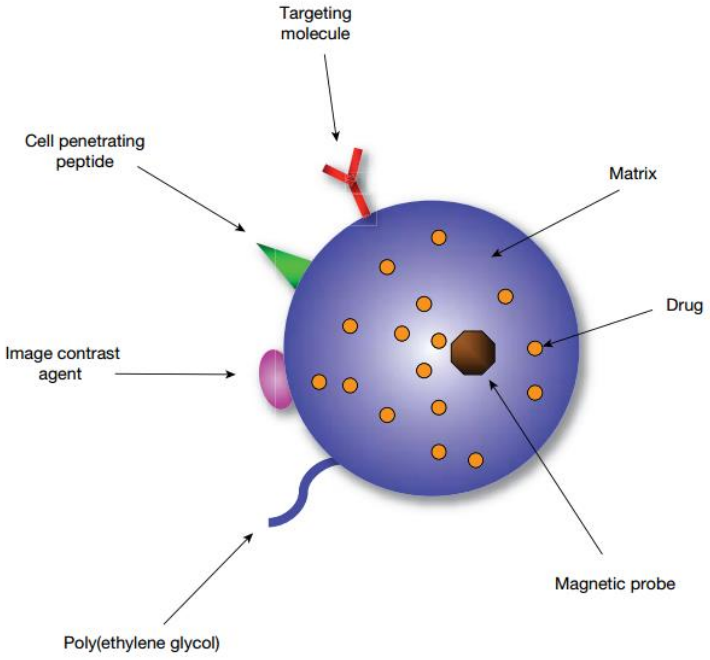

Figure 1-3 – Schematic representation of a multifunctional NP. Adapted from [17].

Although nanomedicine has successfully achieved targeted drug delivery, this would not be possible without the prior identification of novel and specific cell surface markers. These markers are overly expressed in specific tissues or in specific disease-infected tissues and allow an accurate targeting to the tissues in question [28, 30-34, 37].

The multi-functionalization of NPs also offers new opportunities for nanomedicine applications, as it allows a simultaneous conjugation of therapeutic and diagnostic agents in a single approach. In the light of the new nanomedicine advancements, new theranostic approaches are being studied in order to provide more efficient diagnostic, treatment and monitoring of many diseases [21, 22, 32].

Nanomedicine approaches have been studied using several different NPs, like polymeric NPs [26, 29], magnetic NPs [27] and lipid NPs [28, 31, 38]. For the purposes of this work, lipid NPs, in particular solid lipid nanoparticles (SLNs), will be used. They will be more thoroughly discussed in the following sections.

2. State of the Art

In biology, naturally occurring nanostructures have been a source of inspiration for new nanotechnological designs and hybrid-nanostructures made of biological and non-biological, organic and inorganic building blocks. Lipids, with their amphiphilicity, diversity of head and tail chemistry, and antifouling properties that block nonspecific binding to lipid-coated surfaces, provide a powerful toolbox for nanotechnology [18, 19, 21-23].

2.1. Lipid Nanotechnology

The first attempt to incorporate lipophilic drugs in lipid droplets was the parenteral fat emulsion method developed in the 1960s, which is still widely used in the clinic for the parenteral application of poorly water-soluble drugs [23, 39]. But it was only in 1991 that the first generation of lipid NPs, the SLNs, were developed [23, 39-41].

Lipids possess desirable properties for applications in nanomedicine. They are biocompatible, biodegradable and well tolerated all over the body making them very versatile when considering various administration routes. Since the lipids used in the production of lipid nanoparticles naturally exist in the body, their degradation products are easily metabolized by the organism. Therefore lipid nanoparticles for drug delivery applications are associated to little or none systemic cytotoxicity [30, 31, 37, 42-45].

When designing a lipid nanoparticle for drug delivery applications three main types of particle models can be considered: i) solid solution with the drug molecularly dispersed, ii) lipid rich core with drug-enriched shell, and iii) lipid shell with drug-enriched core, as illustrated in figure 2-1. The first model allows for a constant release of drug, as the second and third models enable an immediate and a controlled release, respectively [25, 39-41].

Lipids also have the ability to self-assemble when in aqueous solution into different structures, depending on the lipids used. This enables fast and simple production methods that may also help to lower the cost of NP production and facilitate scale-up of the method used [23, 39, 46, 47].

As previously stated, different types of lipids are used to produce different types of lipid nanoparticles. The three main types of lipid nanoparticles are: i) liposomes and micelles, ii) SLNs, and iii) nanostructured lipid carriers (NLCs) [23, 25, 39, 41, 48, 49]. These different types of lipid nanoparticles are described in detail bellow.

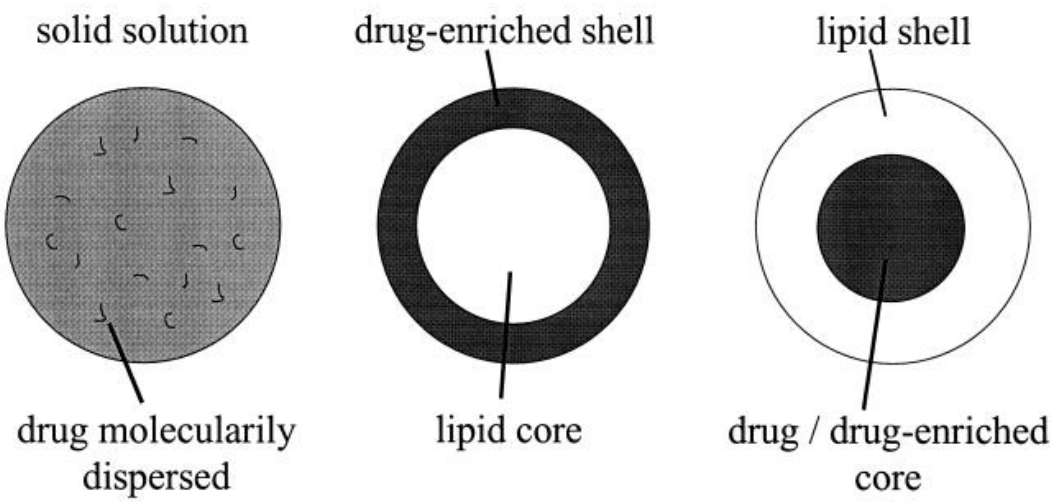

Figure 2-1 - Three drug incorporation models (solid solution model (left), core-shell models with drug-enriched shell (middle) and drug-enriched core (right)). Adapted from [40].

2.1.1. Liposomes and Micelles

Liposomes and micelles are small NPs formed by the self-assembly of amphipilic lipids in aqueous environment. Liposomes are bilayer vesicles, that may be uni- or multi-lamellar, while micelles are monolayer aggregates (figure 2-2) [23, 49-51]. In liposomes the polar heads of the lipids (hydrophilic) are located outwards in the bilayer, faced towards the inner aqueous core and the outer environment. This aqueous core represents an advantage in the use of liposomes for drug delivery as both hydrophilic and lipophilic drugs can be loaded inside the NP, in the core and inside the bilayer membrane of the NP, respectively. In micelles, on the other hand, the polar heads surround the entire lipid aggregate and the apolar tails (hydrophobic) are turned inwards, resulting in a more dense solely hydrophobic structure [49-51].

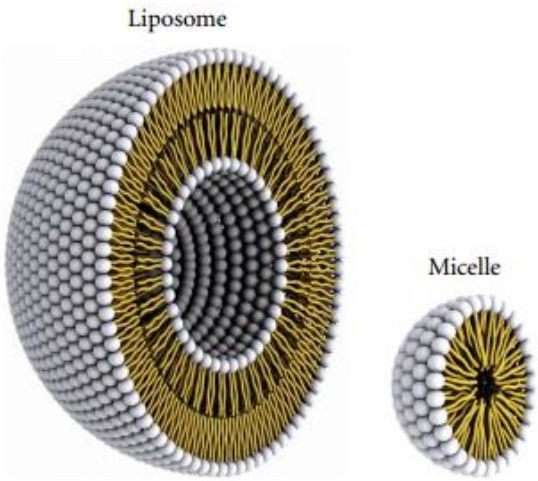

Figure 2-2 – Schematic representation of a liposome (left) and a micelle (right), both transversely sectioned. Adapted from [50].

Both liposomes and micelles may be derived from the hydration of lipid films or from disrupting cellular membranes. However they only form if a specific lipid concentration is achieved in the medium, *i.e.* if the critical micelar concentration (CMC) is reached [23, 49-51].

A key parameter in determining whether liposomes or micelles will be formed is the lipid geometry, since it has great influence in the packing and arranging of the lipids (figure 2-3). Cylindrical lipids, such as phosphatidylcholine, tend to arrange themselves to form lipid bi-layers, favoring liposomal structures, whereas conical lipids, such as lysophosphatidylcholine, tend to form micelles [49-51]. Some lipids, such as arachidonic acid, are known to have an inverted cone geometry and are capable of forming inverse micelles, relying on surfactants to stabilize the hydrophobic tails of the lipid [51, 52].

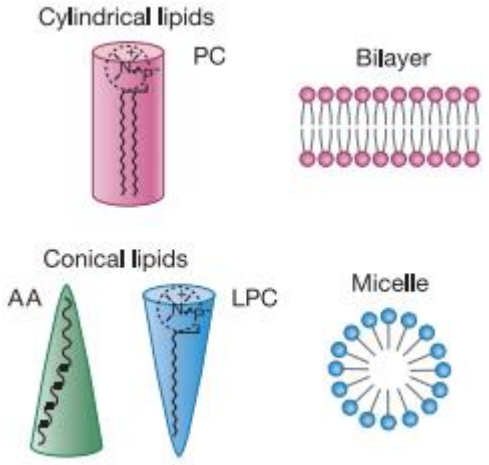

Figure 2-3 – Geometry of phosphatidylcholine (pink), lysophosphatidylcholine (blue), arachidonic acid (green) and their tendency to self-assemble. Adapted from [52].

As previously described, liposomes and micelles are usually produced by self-assembly in aqueous environment and can be easily functionalized recurring to the polar groups existing on their surface. This functionalization can be performed either before or after particle production. It is also possible to incorporate lipids that "react" to specific environments into the lipid layer, making the liposome or micelle responsive to certain conditions, such as low pH [23, 49-51].

Liposomes have found several different applications as NP-based drug delivery systems such as increase skin penetration after topical administration for meloxicam delivery [53], multiple modification for integrin targeting in triple-negative breast cancer [54] and coating with thermosensitive polymers for ultrasound-mediated drug delivery [55].

2.1.2. Solid Lipid Nanoparticles

SLNs are submicron sized nanoparticles, in the range of 50-1000 nm, composed of physiologically tolerated lipid components which are in a solid state at room temperature. These NPs consist of a solid lipid matrix that allows the encapsulation and protection of drugs against degradation and modification of the drug release profile [23, 39-42]. Several different lipids can be used to compose the matrix that has to be stabilized by a surfactant (emulsifier) or combination of surfactants that can highly influence the properties of the resulting particles [30, 43, 46-48, 56].

SLNs are seen as an alternative carrier system to polymeric NPs which is identical to oil-in-water (o/w) emulsions, but where the polymer of the emulsion is replaced by a solid lipid, shown in figure 2-4. Thanks to their structure and composition SLNs combine many of the advantages of polymeric nanoparticles, fat emulsions and liposomes [23, 25, 39, 41, 57, 58]. SLNs allow a controlled release of the encapsulated drug, with excellent biocompatibility and high drug content, increased stability and bioavailability of the bioactive compounds. These NPs are also capable of incorporating hydrophilic and hydrophobic drugs and can be easily subjected to commercial sterilization procedures. However there are a few disadvantages associated with SLNs such as high water content in the dispersions and the possible expulsion of drug during storage due to a shift in crystallization forms [23, 25, 39-41, 57, 59].

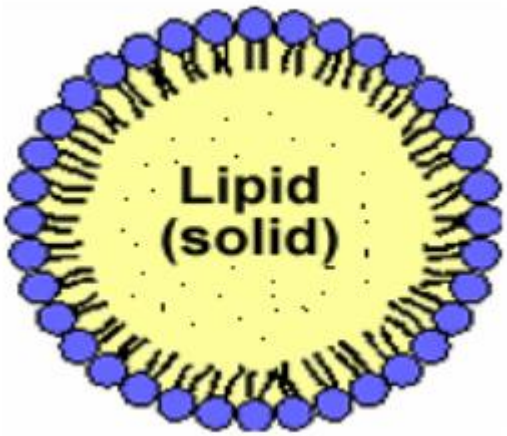

Figure 2-4 – Schematic representation of the structure of a solid lipid nanoparticle (SLN). Adapted from [41].

SLNs can be produced by several different methods from solid lipids, emulsifying agents and water/other solvent. The two most commonly used methods are High Pressure Homogenization (HPH), hot or cold, and w/o/w double emulsion [23, 41, 46, 47, 56]. Both methods are relatively simple and fast, at a relatively low cost, require no special solvents and easily allow scale-up production. HPH may cause drug degradation (high temperatures in hot homogenization) or coalescence (by high pressure) but require no organic solvents of any kind. Whereas double emulsion requires organic solvents but allows the encapsulation of thermo-sensible drugs [46, 47, 56].

SLNs have been used for several different applications by different groups such as to encapsulate SPIONs for controlled drug delivery [60], delivery systems of camptothecin to the brain by intravenous administration [31], oral administration of insulin after modification with stearic acid-actaarginine [61] and coated with chitosan in order to increase drug bioavailability after oral administration [37].

The functionalization of SLNs may be complicated because solid lipids that constitute the NPs possess few exposed polar groups, which are the targets of most functionalization methods [23, 40, 41, 48]. However some success has achieved by using electrostatic layer-by-layer assembly [44, 45], by functionalizing to surfactant instead of the lipids themselves [33, 62], by coating the surface of positively-charged SLNs with polymeric material like chitosan and then functionalizing the polymer [37] and by embedding phospholipids in the SLN and functionalizing them [33, 38].

2.1.3. Nanostructured Lipid Carriers

NLCs are similar to SLNs in several aspects and due to this share many of the same properties and advantages as them (described in the previous section). The main difference between NLCs and SLNs is that the first are produced from a blend of liquid and solid lipids, whereas the latter are produced solely of solid lipids [23, 25, 39, 59]. This compositional variation alters the structure of NP, SLNs tend to form perfect crystals while NLCs inhibit the crystallization process and produce imperfections in the lattices. This mixture of lipids in NLCs can be tailored in order to achieve a pretended nanostructure with the goal to better accommodate the drug or to alter its release profile. NLCs were developed in order to surpass the SLNs potential drug expulsion caused by crystalline form shift, this was achieved by producing a NP without a perfect crystallization of the lipid matrix, as previously described [23, 25, 39].

Three main types of NLCs have been described regarding their structure: i) imperfect type, ii) amorphous type and iii) multiple type, [25, 39, 41, 59] as shown in figure 2-5.

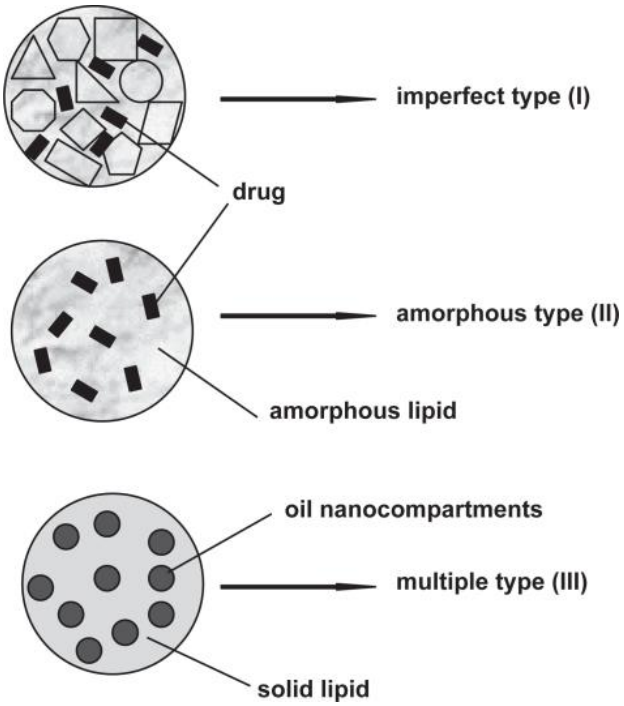

Figure 2-5 – Schematic representation of the three types of NLCs: imperfect type (top), amorphous type (middle) and multiple type (bottom). Adapted from [59].

Imperfect type NLCs have an imperfect structured solid matrix, this is achieved by mixing different lipids (liquid and solid) that cause imperfections in the crystallization of the lipid matrix. These imperfections are what accommodate the drug, additionally mixing small of chemically different liquid lipids increases incompatibility, consequently increasing the number of imperfections and the drug payload. Amorphous type NLCs possess a solid amorphous matrix without any specific structure that prevents drug expulsion caused by crystallization form shift since the matrix is amorphous and not crystalline. This is achieved by mixing solid lipids with special lipids such as isopropylmyristate. Multiple type NLCs consist of multiple oil in fat in water (O/F/W) double emulsions, where the drug is solubilized in the lipophilic phase and its solubility decreases during cooling and storage. Many drugs have higher solubility in liquid lipids than in solid lipids and therefore a higher payload can be obtained using this type of NLC [25, 39, 59].

NLCs have been proposed for applications of different natures such as an attempt to increase cellular uptake by modifying the NLCs with chitosan hydrochlorides [63], optimization of intranasal delivery of artemether [64] and to try and enhance in vitro activity by surpassing drug resistance of Doxorubicin and Ducosahexaenoic acid in cancer cells [65].

2.2. Nanoparticle Functionalization

Nanomedicine has brought a new tool for medical applications laid on the ability to multi-functionalize the drug delivery systems for innumerous purposes. These functionalization can be obtained by different methods, depending on the type of NP and its composition, and designed for different ends, both of which are described in the following sections.

2.2.1. Functionalization Methods

NP functionalization can be achieved by four main approaches (shown in figure 2-6): i) electrostatic attachment, ii) covalent linkage to a NP ligand, iii) attachment to a co-factor bound to the ligand or the NP itself, and iv) direct covalent linkage to the NP surface [27, 33, 34, 66, 67].

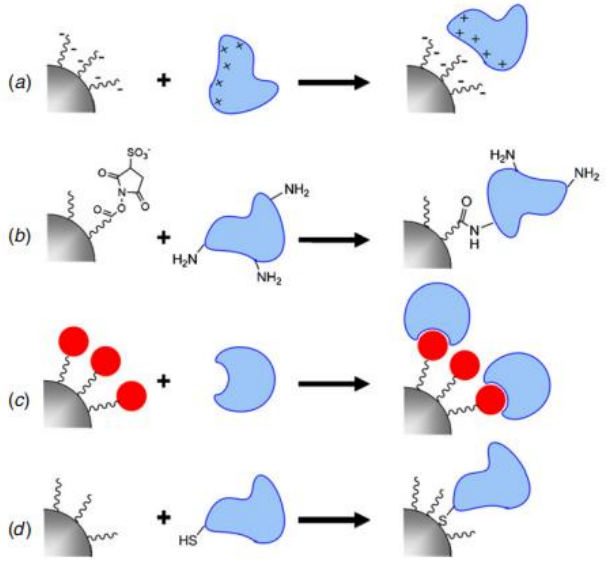

Figure 2-6 – Schematic representation of the four main approaches for NP functionalization: (a) electrostatic attachment, (b) covalent attachment to ligand, (c) attachment to a co-factor and (d) covalent attachment to the NP surface. Adapted from [66].

Electrostatic attachment is the simplest approach that requires no type of chemical reaction consisting of an electrostatic adsorption between differently charged NP and biomolecule. In order to perform this method the surface of the NP has to be electrically charged (negative or positive) so that a biomolecule with the opposite charge can be adsorbed. This method is already routinely used as an electron dense marker in histology [27, 33, 66, 67].

Another general method for NP functionalization is covalent linking to a NP ligand, occurring when a biomolecule (usually a protein or peptide) is able to react with a ligand to form a covalent bound. This linkage is very stable and resistant and is also widely used for surface modification in several NPs applications. The most commonly used functional groups for this reaction are amine and carboxylic acid groups. The method of direct covalent linkage is very similar to this method but instead of the

biomolecule reacting with a functional group on the end of the ligand it reacts with one directly on NP surface [33, 66, 67].

Alternatively, NP functionalization can be achieved attachment to a co-factor. This is usually performed by using specific labeling strategies of bioconjugation: firstly a labeling molecule is attached to the NP surface or NP ligand and after this a second molecule (linked to the desired biomolecule) with great affinity for the label is added creating a stable linking complex. The most commonly used linkage is biotin-streptavidin that allows for up to 4 biotin molecules to be linked to 1 streptavidin and also has a nearly covalent dissociation constant. Note that the antibody conjugation falls into this category of linkage, since the antibody will be linked to the NP and recognize specific epitopes binding only to them [33, 66, 67].

2.2.1.1. Lipid NPs Functionalization

The functionalization of lipid NPs is generally obtained by covalent linkage, directly to the surface or an attached ligand, or by bioconjugation methods. These methods usually imply the use of a lipid "anchor" with an amine, phosphate or carboxylic acid in the head portion, since not all lipids possess functional groups that are capable of functionalization reactions. This lipid anchor is usually pre-functionalized and can be incorporated during NP synthesis or post-synthesis.

Several groups have been able to successfully functionalize SLNs for innumerous nanomedicine applications using the previously described methods, or similar methods with slight variations, as shown in table 2-1.

2.2.2. Functionalization Purposes

A NP functionalization can be performed to achieve a variety of purposes, Table 2-1 shows some examples of SLNs with functionalization for specific applications. Note that the Table 2-1 only shows SLN applications because they are the focus of this work, but the applications described in this section are transversal to all NPs. Most NP surface functionalization aim to: i) decrease identification and elimination by the immune system in the blood stream, ii) enable specific targeting of the NP to the pretended tissue or organ, or iii) facilitate the entry of the NP into the cells [26-29, 32-34, 67].

The coating of the NP with long chain hydrophilic polymers allows the creation of stealth NPs that are not easily recognized by the immune system and therefore have increased circulation time [26, 29, 32, 33]. The use of polyethylene glycol (PEG) chains has been highly described for this type of application and has demonstrated excellent efficacy [26, 29].

Some molecules have the ability to permeate a cell by using specific selective channels in the cellular membrane. These channels could be used as an advantage to increase NP uptake by placing the same molecules in the surface of the NP [33, 34, 66, 67]. This technique has already been

successfully applied, for instance, in the coating NP with polysorbate 80 to help penetrate the Brain-Blood-Barrier (BBB) [30].

NP surface coating with targeting molecules is the most common application of NP surface functionalization, as the molecules are capable of recognizing specific cell membrane markers and attaching only to them, enabling highly specific cell targeting [33, 34, 66, 67]. The use of antibodies as targeting agents is widely described in the literature for targeted drug delivery for example [33, 34].

Table 2-1 – Applications of some specific functionalized SLNs.

Functionalization	Application	Reference
PEG coating	Immune avoidance	[33]
Polysorbate 80	Brain delivery	[30]
Poly-L-Lysine	Transendothelial Permeation	[44]
Polystyrene Sulfonate	Transendothelial Permeation	[44]
Polyacrylic Acid	Transendothelial Permeation	[44]
Poly-L-Lysine	Transendothelial Permeation	[68]
Chitosan coating	Acidic pH resistance	[37]
Heparin	Natural Killer cells targeting	[45]

- This Page was intentionally left blank -

3. Rationale and Strategy of the Thesis

In this work, an approach to attempt targeted therapy and simultaneous imaging is proposed. This study aims to develop a targeted theranostic system for intravenous administration, consisting of the encapsulation of MTX (RA therapeutic drug) and SPIONs (MRI contrast agent) within SLNs. These SLNs are functionalized with a monoclonal antibody (mAb) against the MLS specific cell surface receptor, CD64. A representation of the strategy is shown in figure 3-1.

This work was divided in to two separate phases. Firstly a research on the fundamental basics and the current state of the art was performed as well as a planning of the work to be done in the experimental phase of the work. This phase took place during the first semester of the 2013/2014 school year, from October to January. The second place was accomplished during the second semester of the same school year, from February to June, and consisted mainly of experimental research work, conducted in the department of Chemical Sciences of the Faculty of Pharmacy, University of Porto.

Considering the experimental research work, the first step was NP production and characterization. After the process of optimization, four different formulations were prepared: i) cetyl palmitate SLNs, ii) MTX-loaded cetyl palmitate SLNs, iii) SPIONs-loaded cetyl palmitate SLNs and iv) MTX- and SPIONs-loaded cetyl palmitate SLNs. All of these formulations were then extensively characterized in terms of NP diameter, polydispersion, zeta potential and morphology. The NP content of MTX and SPIONs were also determined. The four formulations were also conjugated with an antibody and its presence was verified and quantified. This extensive characterization enabled comparison of NPs properties and the assessment of each of the formulation's components effect on those properties. Finally *in vitro* assays were performed, using the monocytic cell line THP-1, in order to assess cellular viability and NP's cytotoxicity.

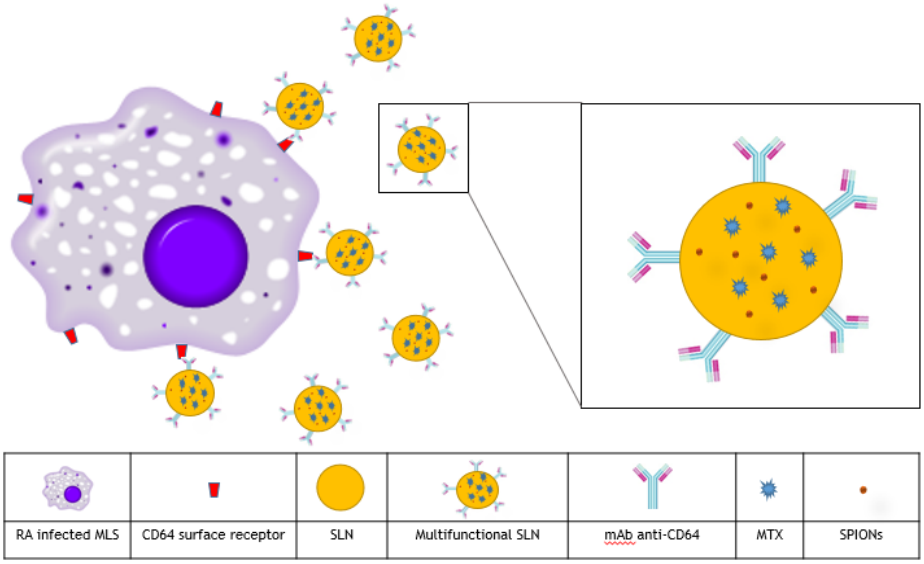

Figure 3-1 – Schematic representation of the proposed strategy for theranostic application in RA.

- This Page was intentionally left blank -

4. Materials and Methods

4.1. Materials

The lipids cetyl palmitate and Witepsol E85 were gently provided by Gattefossé (Saint Priest Cedex, France) and Sasol (Joanesburgo, Gauteng, South Africa), respectively. Stearic acid was purchased from Merck (© Merck KGaA, Darmstadt, Germany). MTX was obtained by courtesy of Excella (Excella GmbH, Feucht, Germany). Iron Oxide Nanocrystals (10 nm) coated with oleic acid and dispersed in chloroform (25 mg/mL) were kindly provided by Ocean Nanotech (Ocean Nanotech Inc., Springdale, AR, USA). Anti-Human CD64 (Fc gamma Receptor 1) antibody solution (1 mg/mL) was purchased from eBioscience (eBioscience Inc., San Diego, CA, USA). LDH Cytotoxicity Detection Kit was from Takara Bio (Takara Bio Inc., Shiga, Japan). Twee 60, dimethyl sulfoxide ACS reagent ≥99.9% (DMSO), dichloromethane (ACS reagent, ≥99.5% contains 50 ppm amylene as stabilize), ethyl acetate (ACS reagent, ≥99.5%), 2-morpholinoethanesulfonic acid low moisture content, ≥99% (MES), 1-ethyl-3-(3-dimethylaminopropyl) carbodiimide hydrochloride purum, ≥98.0% (EDC), N-hydroxysulfosuccinimide 98% (NHS), Thiazolyl Blue Tetrazolium Bromide 98% (MTT), Triton™ X-100 for molecular biology, Trypan Blue powder and phorbol 12-myristate 13-acetate (PMA) were purchased from Sigma-Aldrich (St. Luis, MO, USA). Dulbecco's Modified Eagle's Medium (DMEM), Dulbecco's phosphate buffer saline 10x pH 7.4 (PBS), fetal bovine serum (FBS), Penicillin-Streptomycinm and Fungizone ® Antimycotic were purchased from Gibco® (Invitrogen Corporation, Paisley, UK). Aqueous solutions were prepared with double-deionized water (Arium Pro, Sartorius AG, Göttingen, Germany). THP-1 (ATCC® TIB-202™) cells were generously provided by Professor Susana Santos and Doctor Marta Freitas, INEB

4.2. Methods

4.2.1. Preparation of Multifunctional Nanoparticles

4.2.1.1. Optimization of Nanoparticle production method

In the first attempt of NP production both cetyl palmitate and Witepsol E85 were used in an organic solvent-free emulsification-sonication method that combined high shear homogenization and ultra-sonication. As standard procedure, 500 mg of solid lipid (cetyl palmitate and Witepsol E85) and 100 mg of surfactant (Tween 60) were heated to 70ºC, in order to fuse the lipids. After the lipids were totally fused, 4.400 mL of water at 70ºC were added to the fused lipid-surfactant mixture, and the resulting solution was immediately homogenized with a high-shear homogenizer (YSTRAL GMBH X10/20-E3, Ballrechten-Dottingen, Germany) for 30 seconds at 12000 rpms to produce a lipid-in-water micro-emulsion. This micro-emulsion was afterwards re-homogenized using a probe-type sonicator (model VCX-130 with a VC 18 probe, Sonics&Materials Inc., Newtown, CT, USA) for 5 minutes at 80%

amplitude to produce the NPs. The resulting NP suspension was stored in glass flasks at room temperature until further use.

Table 4-1 - Physicochemical properties of the NP formulations. Size, PdI and Zeta potential for all the formulations considering both Witepsol E85 and cetyl palmitate SLNs for different homogenization and sonication times.

Lipid used in SLN	Homogenization time (sec)	Sonication time (min)	Size (nm)	PdI	Zeta Potential (mV)
Witepsol E85	30	5	798.5 ± 16.8	0.372 ± 0.004	-34.27 ± 0.66
Witepsol E85	30	10	954.5 ± 3.40	0.372 ± 0.016	-27.14 ± 0.96
Witepsol E85	30	15	762.9 ± 37.5	0.350 ± 0.022	-28,04 ± 1,05
Witepsol E85	60	5	781.1 ± 125.8	0.334 ± 0.019	-22.39 ± 0.87
Witepsol E85	60	10	639.3 ± 68.1	0.346 ± 0.003	-26.03 ± 0.64
Witepsol E85	60	15	338.3 ± 9.6	0.334 ± 0.026	-29.02 ± 1.14
Witepsol E85	120	5	729.2 ± 68.3	0.388 ± 0.006	-28.31 ± 0.76
Witepsol E85	120	10	661.9 ± 30.6	0.333 ± 0.030	-28.16 ± 0.95
Witepsol E85	120	15	536.0 ± 21.6	0.379 ± 0.004	-21.99 ± 2.69
Cetyl Palmitate	30	5	466.4 ± 16.7	0.248 ± 0.019	-36.67 ± 0.78
Cetyl Palmitate	30	10	333.0 ± 8.2	0.280 ± 0.010	-36.18 ± 0.75
Cetyl Palmitate	30	15	471.2 ± 7.8	0.286 ± 0.010	-36.35 ± 0.92
Cetyl Palmitate	60	5	455.7 ± 3.6	0.277 ± 0.008	-36.52 ± 0.83
Cetyl Palmitate	60	10	426.2 ± 2.2	0.277 ± 0.004	-34.02 ± 0.69
Cetyl Palmitate	60	15	430.0 ± 5.9	0.247 ± 0.011	-33.57 ± 1.86
Cetyl Palmitate	120	5	397.3 ± 6.3	0.234 ± 0.015	-31.71 ± 1.04
Cetyl Palmitate	120	10	437.3 ± 7.1	0.252 ± 0.010	-29.20 ± 1.01
Cetyl Palmitate	120	15	415.3 ± 7.1	0.246 ± 0.017	-37.13 ± 0.49

In an attempt to better understand the effects of the homogenization process in NPs properties new NPs were prepared, using the same method that was previously described but increasing both homogenization and sonication times. It was found that increasing the homogenization times (30 seconds, 1 minute and 2 minutes) or the sonication times (5 minutes, 10 minutes and 15 minutes)

resulted in little changes to the NP properties and so no alterations were done to the original method (table 4-1).

To later facilitate NP functionalization the number of available functional groups, in particular carboxylic terminal groups, on the NP surface should be increased as much as possible. In order to achieve, this the addition of a fatty acid was proposed. Fatty acids have long hydrophobic chains that enable an easy integration into the SLN matrix and possess a terminal carboxylic acid group that could be used for antibody conjugation. Two fatty acids were chosen and assessed (Table 4-2) for this: i) stearic acid (an 18-C long saturated fatty acid) and ii) oleic acid (an 18-C long unsaturated acid fatty acid). The results showed that the NP formulation with more promising characteristics were composed of cetyl palmitate and stearic acid and, therefore, the other formulations were discarded at this point. To further optimize the cetyl palmitate/stearic acid formulation several proportions of acid were used (2.5%, 5%, 7.5% and 10%) and best properties were obtained using 7.5% (regarding total formulation weight) of stearic acid (Table 4-3).

Table 4-2 - Physicochemical properties of the NP formulations. Size, PdI and Zeta potential for all the formulations considering both Witepsol E85 and cetyl palmitate SLNs with oleic and stearic acid.

Lipid used in SLN	Fatty acid	Size (nm)	PdI	Zeta Potential (mV)
Witepsol E85	Oleic acid	607.0 ± 18.1	0.358 ± 0.008	-41.10 ± 3.10
Witepsol E85	Stearic acid	660.9 ± 56.0	0.309 ± 0.020	-36.93 ± 1.42
Cetyl palmitate	Oleic acid	426.6 ± 150.3	0.241 ± 0.025	-39.08 ± 1,21
Cetyl palmitate	Stearic acid	408.6 ± 16.4	0.229 ± 0.031	-41.11 ± 0.35

Table 4-3 - Physicochemical properties of the NP formulations. Size, PdI and Zeta potential for all the formulations considering cetyl palmitate SLNs with stearic acid at different %.

Lipid used in SLN	Stearic acid %	Size (nm)	PdI	Zeta Potential (mV)
Cetyl palmitate	2.5%	607.0 ± 18.1	0.358 ± 0.008	-28.84 ± 2.33
Cetyl palmitate	5.0%	660.9 ± 56.0	0.309 ± 0.020	-34.58 ± 1.50
Cetyl palmitate	7.5%	426.6 ± 150.3	0.241 ± 0.025	-40.04 ± 0.96
Cetyl palmitate	10.0%	408.6 ± 16.4	0.229 ± 0.031	-39.62 ± 1.45

The selected formulation (cetyl palmitate with 7.5% stearic acid) was still presenting dimensions that were too large for the pretended application. On a first attempt to reduce NP diameter the NP suspension were filtrated (using disposable syringes and cellulose filters with several pore sizes). Filtration greatly improved NP diameter but it was shown to retain a large amount of NPs in the filters, causing a large amount of mass loss that would be translated in the future to large drug loss. Because of this issue filtration was discarded from the process. In another attempt to reduce NP size a decrease in total lipid quantity (600 mg to 400 mg of total formulation) and an increase in the

lipid/surfactant proportion (16%, 20%, 25%, 30% and 35% of the formulation total) was considered (the latter results can be observed in Table 4-4). The formulation that presented the best NP characteristics was composed of 400 mg of total mass with theoretical 35% of surfactant.

Table 4-4 - Physicochemical properties of the NP formulations. Size, PdI and Zeta potential for all the formulations for cetyl palmitate SLNs with surfactant at different %.

Lipid used in SLN	Surfactant (%)	Size (nm)	PdI	Zeta Potential (mV)
Cetyl palmitate	16%	434.2 ± 12.8	0.284 ± 0.015	-37.65 ± 1.31
Cetyl palmitate	20%	340.3 ± 5.3	0.231 ± 0.007	-49.78 ± 0.70
Cetyl palmitate	25%	255.6 ± 4.0	0.206 ± 0.008	-47.27 ± 1.19
Cetyl palmitate	30%	214.4 ± 3.6	0.200 ± 0.008	-46.78 ± 0.61
Cetyl palmitate	35%	164.6 ± 1.9	0.189 ± 0.008	-44.33 ± 1.30

4.2.1.2. Definitive Nanoparticle production method

SLNs composed of cetyl palmitate and stearic acid were prepared by an organic solvent-free emulsification-sonication method that combined high shear homogenization and ultra-sonication (figure 4-1). As standard procedure, 230 mg of cetyl palmitate, 30 mg of stearic acid and 140 mg of Tween 60 were heated to 70ºC (temperature above the fusion point of all the lipids in the mixture), in order to fuse the lipids. 4.400 mL of water at 70ºC was added to fused lipid-surfactant mixture and the resulting solution was immediately homogenized with a High-shear Homogenizer (YSTRAL GMBH X10/20-E3, Ballrechten-Dottingen, Germany) for 30 seconds at 12000 rpms to produce a lipid-in-water micro-emulsion. This micro-emulsion was afterwards re-homogenized using a probe-type sonicator (model VCX-130 with a VC 18 probe, Sonics&Materials Inc., Newtown, CT, USA) for 5 minutes at 80% amplitude to produce the NPs. The resulting NP suspension was stored in glass flasks at room temperature until further use.

The encapsulation of both MTX and SPIONs was achieved during the production method [35]. 4 mg of MTX were added prior to the lipid fusing and dissolved, as much as possible, in fused solid lipid + surfactant mixture. 40 µl of SPION dispersion were added after the lipid fusion and before the addition of the water.

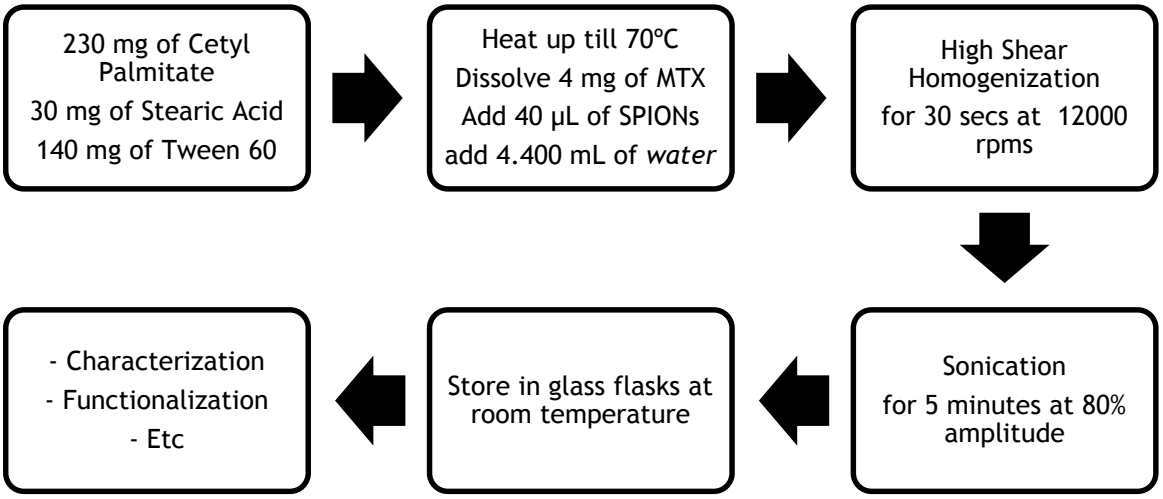

Figure 4-1 – Schematic representation of the NP preparation procedure.

Four different formulations were prepared: i) SLN-Placebo (cetyl palmitate NPs not containing MTX or SPIONs), ii) SLN-MTX (cetyl palmitate NPs containing only MTX), iii) SLN-SPIONs (cetyl palmitate containing only SPIONs) and iv) SLN-MTX/SPIONs (cetyl palmitate containing both MTX and SPIONs).

4.2.1.3. Antibody conjugation to the Solid Lipid Nanoparticles

As previously stated, the SLN were further functionalized with an anti-CD64 antibody that is able to recognize macrophage's CD64 (present in the macrophage cell membrane and over expressed in RA). This recognition is performed by the antibody's Fc region and because of this any attempt of antibody conjugation must be done through the antibody's Fab fragment in order to maintain its functionality [69]. Considering this, the conjugation reaction performed in two steps: i) the NP's carboxylic groups (present in the stearic acid that was integrated into the SLN matrix) were activated in the presence of EDC and NHS, and ii) the antibody's primary amine (Fab fragment) reacted with the activated carboxylic group to form a stable amide bound between the SLN surface and the antibody [35].

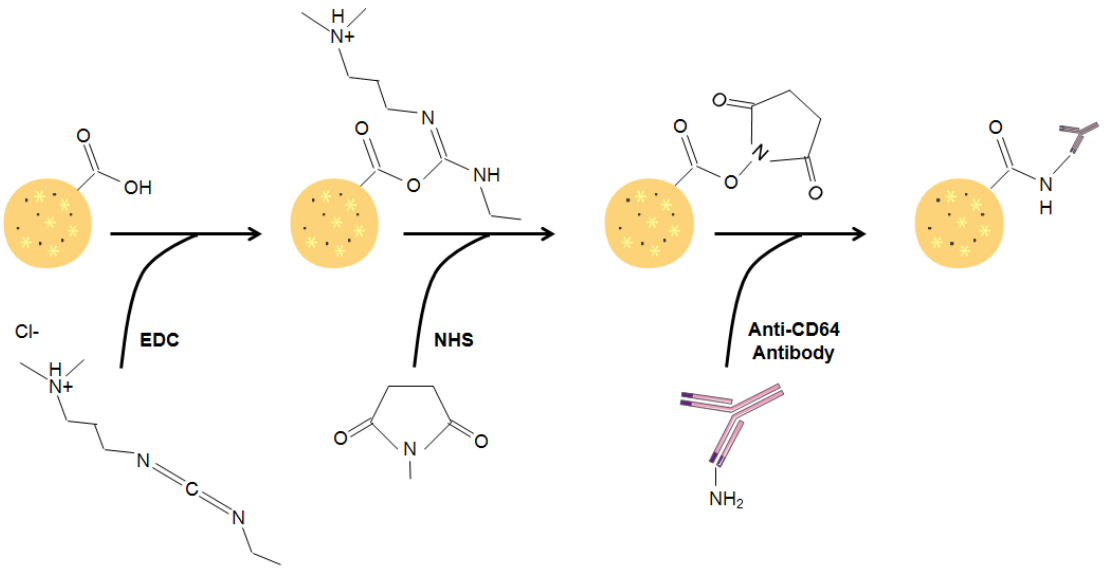

Figure 4-2 – Schematic representation of the NP functionalization procedure's several reactions. Adapted from [35].

The NP formulations were diluted in 10 mL of MES buffer, pH 5.0 (this value of pH ensures maximum EDC attachment to carboxylic groups), so that the final concentration is 10 mg of NPs per mL of buffer. The NPs were then activated by adding 1 mL of 0.1 M EDC and 1 mL of 0.7 M NHS (both dissolved in MES buffer, pH 5.0) to the previously prepared suspension. The NP suspension was then kept at room temperature under moderate stirring for 1h. 1 mL of the activated-NP suspension was transferred to an Eppendorf® tube and 10 µL of the anti-CD64 antibody solution were added to the latter. The resulting suspensions were then homogenized with a vortex and incubated at 4ºC for 24h. The functionalized NPs were then stored at 4ºC until further usage [35].

4.2.2. Nanoparticle characterization

4.2.2.1. Dynamic light scattering and phase analysis light scattering

Dynamic light scattering (DLS), also known as photon correlation spectroscopy or quasi-elastic light scattering, is a commonly used technique for the determination of size distribution profiles in the sub-micron range. The technique is based on the Brownian motion, that is, particles and molecules are in constant random motion and the speed at which they move is related to their size (smaller particles move faster that larger ones). The movement speed can be determined by measuring the changes of the scattered intensity at a specific angle through time and, taking into account the temperature of the suspension, the hydrodynamic radius of the NPs can be determined was well as its size distribution [70].

Zeta potential is a physical property related to the charge of a particle and can be used to infer on the stability of a suspension or system. When the modulus of the zeta potential is high the particles tend to repel each other, due to strong electric charges, and hence do not tend to agglomerate. However if the modulus is low the electric charges will not have enough force to repel each other and the particles will have a tendency to form agglomerates. The zeta potential can be measured by phase analysis light scattering (PALS), that relies on applying an electric field to the suspension that will force the particles to move the electrodes depending on their charge. The movement speed of the particles is dependent of the field applied and of the particles zeta potential, since the field is known the zeta potential can be easily determined [71].

The NP formulations were characterized in terms of particle diameter, diameter distribuition profile (polydispersity index - PdI) and zeta potential by upper mentioned techniques. Mean diameter and PdI were determined by DLS using a 90Plus Particle Size Analyzer (Brookhaven Instruments Corporation, Holtsville, NY, USA) and the zeta potential was assessed by PALS using a ZetaPALS Zeta Potential Analyzer (Brookhaven Instruments Corporation, Holtsville, NY, USA), at 660 nm, at 20ºC with a detection angle of 90º. The formulations were previously diluted in water, the non-conjugated NPs 400x and the conjugated NPs 4x, to achieve a final concentration of 250 µg of NP per mL for all formulations. All measurements were performed with three independent batches of NPs, with six runs each.

4.2.2.2. Transmission Electron Microscopy

Transmission electron microscopy (TEM) uses an electron beam to illuminate ultra-thin samples (under 0.5 µm thick). The electrons interact with the sample and those that pass through it are collected by a system of electromagnetic lenses that greatly magnifies and focus the image. The image formed is collected and displayed in an imaging device, such as a florescent screen, on a layer of photographic film or, more commonly, its detected by a sensor such as a CDD camera.

Prior to the TEM analysis, the non-conjugated NP suspensions were diluted 100X in *water* to achieve a 1 mg/mL concentration, since the conjugated NPs were already at this concentration (result of the functionalization procedure). Samples were prepared by placing 10 µL of NP dispersion on a copper-mesh grid (one grid for each different sample) and after 2 minutes the excess of suspension was removed with filter paper. As a contrasting agent, 10 µL of 0.75% uranyl acetate solution were placed on the grid and after 30 seconds the excess was removed using filter paper. The grids were after observed in a JEM-1400 Transmission Electron Microscope (JEOL Ltd.), with an accelerating voltage of 80 kV.

4.2.2.3. MTX Quantification

Spectrophotometry is a technique that allows for a quantitative measurement of the amount of radiation that a samples absorbs. A beam of light (visible or not) passes through a sample and the amount of light that reach the detector is measured. The amount of light that a molecule absorbs, at a specific wavelength, can then be used to determine the amount of that molecule that is present in the solution. UV/Vis spectrophotometry was used to determine the amount of MTX present in the formulations using an indirect method, *i.e.* the amount of drug that was present outside the NPs was dosed, and the association efficiency was determined by subtracting the amount of MTX that remained in the aqueous phase to total amount of MTX (equation 1).

$$(1)\ \text{Association efficiency}\ (\%) = \frac{\text{Total amount of MTX} - \text{Amount of MTX in the supernatant}}{\text{Total amount of MTX}} \times 100$$

Firstly the NP suspensions were diluted 200x and filtrated with Amicon ® Ultra Centrifugal Filters Ultracell-50 kDa (EMD Millipore, Darmstadt, Germany) at 3500 G for 30 minutes using a Heraeus™ Multifuge™ X1R centrifuge (Thermo Scientific, Waltham, MA, USA). The resulting supernatant was collected for MTX quantification by spectrophotometry. The absorbance of the supernatant was then read using a V-660 UV/Vis Spectrophotometer (Jasco Inc., Easton, MD, USA), and the values of the absorbance were registered at 299 nm wavelength (MTX absorbance peak). The readings of each sample, containing MTX, were corrected using the supernatant resulting from filtration of the respective formulation without MTX (SLN-placebo was used as baseline for SLN-MTX, and SLN-SPIONs was used as baseline for SLN-MTX/SPIONs) in order to minimize formulation interferences. Each sample reading was performed in triplicate (each from an independent batch of NP formulations).

A calibration curve was constructed using standard solutions of MTX with the final concentrations of 0.000625, 0.00125, 0.0025, 0.005, 0.010, 0.020, 0.030 and 0.040 mg/mL. In order to minimize reading interferences these standard solutions were prepared in the supernatant resulting from the previously described filtration of SLN-placebo NP suspension.

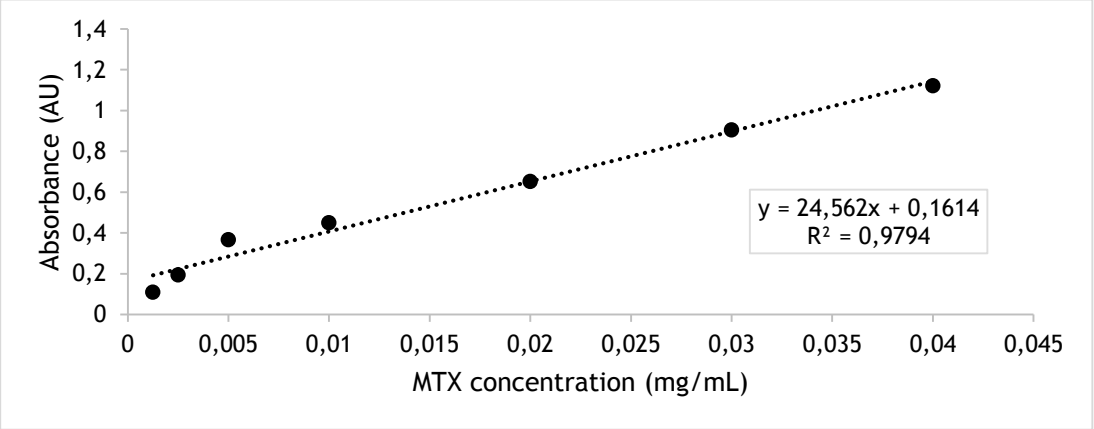

Figure 4-3 – Standard curve for MTX quantification using spectrophotometry.

4.2.2.4. Fourier Transform Infrared spectroscopy

Fourier transform infrared (FT-IR) spectroscopy is a technique that allows the identification of samples specific molecular bonds that can used to identify components. It uses an infrared beam that passes through the sample and collects an absorbance/transmittance spectrum whose peaks correspond to the frequencies of vibrations between the bonds of the chemical elements present in the sample. Because each different material is a unique combination of atoms, the infrared spectrum works as molecule fingerprint making it possible to identify, with great certainty, the components of the sample[72]. FT-IR analysis proved extremely useful in determining the presence of both MTX and antibody within the NP formulations.

Prior to FT-IR analysis the NP formulations were lyophilized, firstly 1 mL of NP suspension was frozen at -80ºC for 30 minutes and after place in a Bench Top Pro with Omnitronics (SP Scientific, Warminster, PA, USA) at -80ºC at 150 mTorr for 18h. The resulting powders were then characterized by FT-IR analysis, using a Frontier FT-IR Spectrometer with Universal ATR Sampling Accessory (PerkinElmer, Waltham, MA, USA). Each of the infrared spectrum was collect with 32-scans with 4 cm^{-1} resolution in the mid-infrared region (3700 to 600 cm^{-1}).

4.2.2.5. Antibody Quantification

The amount of antibody conjugated to the NPs was indirectly determined by quantifying the total amount of protein of the formulation that was not linked to the NPs. In order to separate the free antibody from the NP-conjugated antibody the conjugated NP suspension was centrifuged at 33000 G for 5h, and the supernatant was carefully collected.

The antibody was after quantified using a colorimetric method with the Thermo Scientific™ Coomassie (Bradford) Protein Assay Kit. This kit allows for a quick and viable quantification of the total amount of protein present – when Coomassie dye binds to a protein, in acidic medium, it produces an immediate color change from brown to blue, resulting in a shift of the maximum absorbance peak from 465 nm to 595 nm [73].

Firstly a calibration curve for the amount of protein was constructed (Figure 4-3) using standard bovine serum albumin (BSA) solutions with concentrations of 25, 20, 15, 10, 5, 2.5 and 0 μg/mL of BSA in PBS. In order to measure the absorbance of both standard solutions and samples, the micro microplate protocol was used. 150 μL of the standard solutions/samples were transferred to a 96-well plate, in triplicate, and 150 μL of the coomassie reagent was added to those plates. The 96-well plate was stirred for 30 seconds and left to incubate at room temperature protected from the light. The plate was then read at 595 nm using a Synergy™ HT Multi-mode Microplate Reader (Biotek Instruments Inc., Winooski, VT, USA).

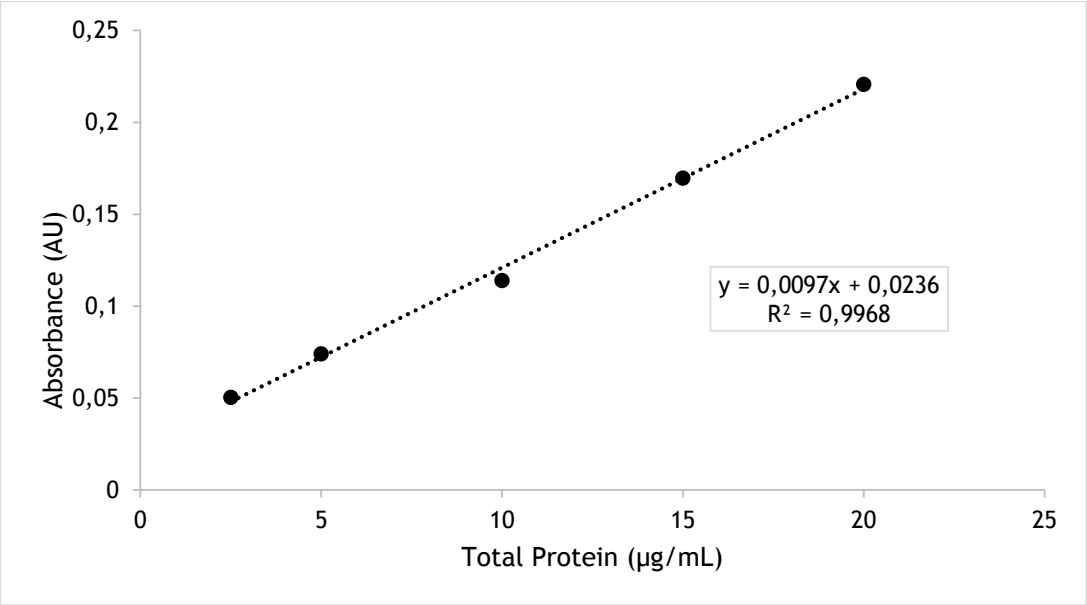

Figure 4-4 – Standard curve for total protein quantification using spectrophotometry.

The total amount of protein present in the supernatant (free antibody) was then calculated using the previously constructed calibration curve, and the conjugation efficiency was determined using Equation 2.

$$(2)\ \text{Conjugation efficiency}\ (\%) = \frac{\text{Total amount of antibody} - \text{Amount of free antibody}}{\text{Total amount of antibody}} \times 100$$

4.2.3. *In Vitro* Studies

THP-1 (ATCC® TIB-202™), cultured in DMEM medium supplemented with 10% FBS and 1% Penicillin-Streptomycin, incubated in a humidified environment at 37ºC with 5% CO_2 enriched atmosphere. To perform subculture the cells were collected and centrifuged at 300 G and re-suspended in fresh medium and counted using a Neubauer chamber, diluted in a Trypan Blue solution 0.4% (w/v) in PBS in order to distinguish viable cells from the non-viable ones. The cells were then transferred to a new culture flask to achieve o final cellular concentration of $2*10^5$ cells/mL and the total amount of medium was adjusted to the flask size [74].

4.2.3.1. MTT Assay

The MTT assay is a colorimetric assay that enables the assessment of cellular metabolism and inference on cellular viability. It measures the activity of cellular enzymes that are capable of reducing the thiazol blue tetrazolium bromide (MTT) substrate to form insoluble formazan crystals, which present a purple color instead of blue [75]. Prior to the assay a calibration curve was

constructed to determine the optimal cellular seeding density to be used in the assay, *i.e.*, ensure that the measurements fall within the linear detection range. To construct the curve 200 μL of cellular suspensions at 1000, 10000, 20000, 40000, 60000, 80000, 100000, 120000, 150000 and 200000 cells/mL were seeded into a 96-well tissue culture test plates (Orange Scientific Products, Belgium), in triplicate. The cellular suspensions were in DMEM culture medium supplemented with 10% FBS and 1% Penicillin-Streptomycin, with 0.02 μL/mL of PMA (a differentiation agent that causes the THP-1 cells to adhere to plate). The 96-well plates were incubated at 37ºC with 5% CO_2 enriched atmosphere for 24h. The medium was then removed and replaced with 200 μL of fresh warm DMEM culture medium supplemented with 10% FBS and 1% Penicillin-Streptomycin and incubated at 37ºC with 5% CO_2 enriched atmosphere for another 24h. After 24h of incubation the medium was removed, 5 mg/mL MTT dye solution in PBS were diluted in culture medium to achieve a final concentration of 0.5 mg/mL and 200 μL of the latter solution were added to each well. The 96-well plate was incubated at 37ºC with 5% CO_2 enriched atmosphere, protected from the light for 4h. After 4h the plate was removed from the incubator, the MTT solution was removed and 200 μL of DMSO were added, to dissolve the formazan crystals. The absorbance was then read by using a Synergy™ HT Multi-mode Microplate Reader (Biotek Instruments, USA) at 590 nm and 630 nm, the latter was used for background subtraction. The obtained results were used to construct a calibration curve (Figure 4-4), and the cellular density of $60x10^3$ cells/mL was chosen as the optimal density since was registered approximately in the middle of linear portion of the curve.

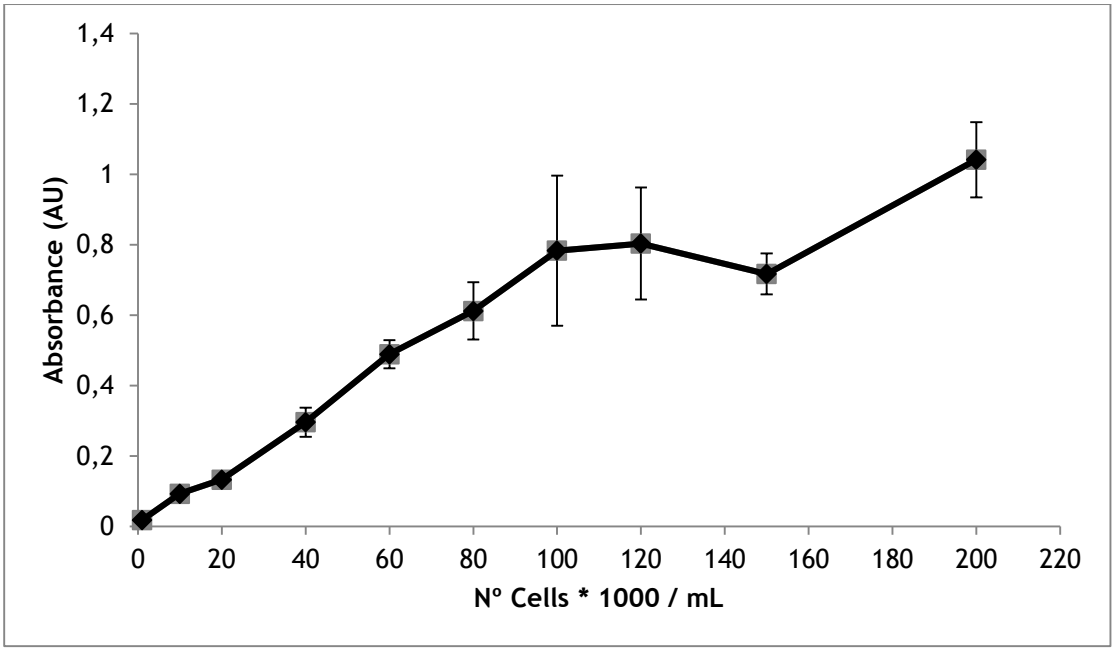

Figure 4-5 – Standard calibration curve for cell seeding density on the MTX assay. Mean Values ± Standard deviation values shown, with n=3.

Once the optimal cellular density was determined for the MTT assay, the assay was performed with all formulations of the produced NPs, at different concentrations, on differentiated THP-1 cells. 200 μL of cellular suspensions ($60x10^3$ cells/mL in DMEM culture medium supplemented with 10% FBS

and 1% Penicillin-Streptomycin, with 0.02 μL/mL of PMA) were seeded into a 96-well tissue culture test plates (Orange Scientific Products, Braine-l'Alleud, Belgium), in quintuplicate. The 96-well plates were incubated at 37ºC with 5% CO_2 enriched atmosphere for 24h, after this the medium was removed and replaced with 200 μL of fresh warm DMEM culture medium (supplemented with 10% FBS and 1% Penicillin-Streptomycin) and incubated at 37ºC with 5% CO_2 enriched atmosphere for another 24h. After 24h of incubation the medium was removed and 200 μL (100 μL of medium + 100 μL of PBS) of NP suspension were added with the final concentrations of (0.05, 0.5, 5, 50 and 500 μg/mL). A positive control (100 μL of medium + 100 μL of PBS) and negative control (200 μL of Triton™ X-100 2% (w/v) in PBS) as well as a control of free MTX (at the same relative concentrations as the NP suspensions) were also include to normalize and better compare results. After 24h of incubation at 37ºC with 5% CO_2 enriched atmosphere, the MTX assay was performed as previously described. Cellular viability was then determined using equation 3.

$$(3)\ \text{Viability}\ (\%) = \frac{\text{Experimental Value} - \text{Negative Control}}{\text{Positive Control} - \text{Negative Control}} \times 100$$

4.2.3.2. LDH Assay

Lactate dehydrogenase (LDH) is a cytosolic enzyme present in a wide variety of cellular types that catalyzes the metabolism of lactate. This enzyme is released into the culture medium if the cellular membrane is damaged and can, therefore, be used to assess cytotoxicity levels and cellular death by membrane lysis. It can be easily quantified by using the LDH Cytotoxicity Detection kit that works by quantifying the amount of red formazan product formed in the cellular supernatant after incubation with the kit's reaction mixture. The level of formazan formed is directly proportional to the amount of LDH released into the medium and, therefore, its activity can be determined [76].

The LDH assay was done in parallel with the MTT assay, since they share several steps, namely the 96-well plate seeding and differentiation and the 24h of incubation at 37ºC with 5% CO2 enriched atmosphere, either with the medium and with NP dispersions at various concentrations. After the incubation with the free MTX or NP dispersions, the medium was removed and transferred to another 96-well plate to perform the LDH assay. The resulting 96-well plates were centrifuged for 10 minutes at 250 g at room temperature. Carefully, not to disturb the resulting pellet, 100 μL of the supernatant from each well were transferred to another 96-well plate. 100 μL of LDH reaction mixture were then added to each well and the plates were incubated at room temperature, protected from light for 20 minutes. After incubation the absorbance was then read using a SynergyTM HT Multi-mode Microplate Reader (Biotek Instruments, Highland Park, Winooski, USA) at 490 nm and 630 nm, the latter was used for background subtraction. The NP cytotoxicity was determined using Equation (4). It is important to note that since a cytotoxicity assay was performed, the negative control used were the cells culture with medium+PBS and the positive control were the cells cultured with Triton™.

$$(4)\ \text{Cytotoxicity}\ (\%) = \frac{\text{Experimental Value} - \text{Negative Control}}{\text{Positive Control} - \text{Negative Control}} \times 100$$

4.2.4. Statistical analysis

Statistical analyses were performed using IBM® SPSS® Statistics (SPSS 22.0, USA). Results are presented as mean value ± standard deviation from a minimum of three independent experiments. Two-tailed student's t-test and one-way analysis of variance (ANOVA) were performed to compare multiple groups of independent samples, respectively. When the groups showed significant statistical difference ($p \leq 0.05$), the differences between the respective groups were compared with a post-hoc test (Tukey, $p \leq 0.05$). Paired (non-independent) samples were analyzed with a paired-samples two-tailed student's t-test. Differences were once again considered significant at $p \leq 0.05$.

- This Page was intentionally left blank -

5. Results and discussion

As previously stated four different formulations were prepared: i) cetyl palmitate SLNs, ii) MTX-loaded cetyl palmitate SLNs, iii) SPIONs-loaded cetyl palmitate SLNs and iv) MTX- and SPIONs-loaded cetyl palmitate SLNs. For the formulations to the effective in the treatment and diagnostics of AR it is of the up most importance to ensure that both the therapeutic and the imaging agents, MTX and SPIONs respectively, are properly integrated into the NPs [22, 25, 39, 42].

Indications that this integration occurred were seen immediately after NP production without any kind of complex characterization. The NP formulations presented distinct color depending if they were placebo SLN or encapsulated with one or both of agents, as shown in Figure 5-1. The difference between the colors of the formulations was the first indication that the encapsulation of both MTX and SPIONs, separately and simultaneously, occurred during the production phase.

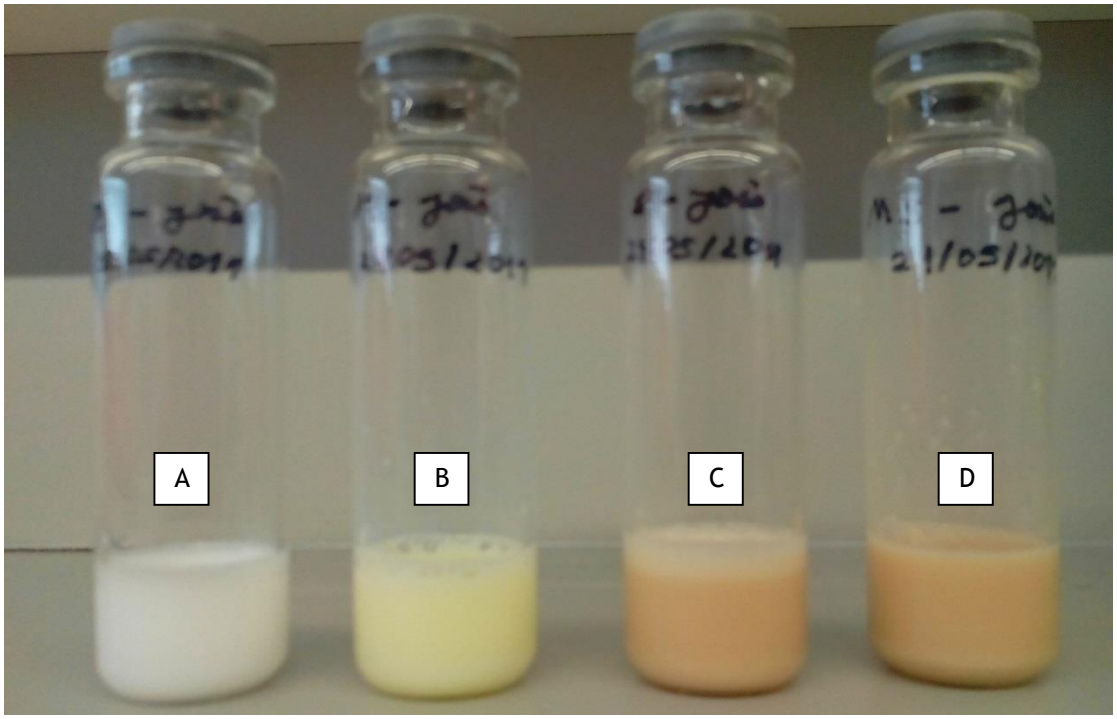

Figure 5-1 – Multifunctional NP formulations prepared by an organic solvent-free emulsification-sonication method that combined high shear homogenization and ultra-sonication. (A) cetyl palmitate SLNs, (B) MTX-loaded cetyl palmitate SLNs, (C) SPIONs-loaded cetyl palmitate SLNs and (D) MTX- and SPIONs-loaded cetyl palmitate SLNs.

5.1. Nanoparticle characterization

The properties and characteristics of the NPs influence the formulation stability and can also influence their future interactions with cells and tissues, so they were extensively characterized in terms of NP size, PdI, Zeta potential, MTX and SPIONs encapsulation as well as antibody-conjugation. These characteristics are summarized in Table 2-1 for all NP formulations.

Table 5-1 – Physicochemical properties of the NP formulations. Size, PdI and Zeta potential for all the formulations and MTX association for the MTX-loaded and MTX- and SPIONs-loaded SLN prior to NP functionalization and post-functionalization.

Formulation	Size (nm)	PdI	Zeta Potential (mV)	MTX Association (%)
SLN	161.00 ± 2.73 [a]	0.190 ± 0.008 [a]	-39.58 ± 0.87 [a]	- - -
SLN + MTX	173.97 ± 3.40 [a]	0.195 ± 0.013 [a]	-35.06 ± 1.09 [a]	98.23 ± 8.82
SLN + SPIONs	243.97 + 4.00 [a]	0.254 ± 0.008	-28-65 ± 0.74 [a]	- - -
SLN + MTS + SPIONs	227.60 ± 3.67 [a]	0.256 ± 0.006	-24.73 ± 0.55 [a]	105.68 ± 4.75
SLN + Anti-CD64	113.67 ± 2.93 [c]	0.081 ± 0.019 [c]	-22.95 ± 0.80 [c]	- - -
SLN + MTX + Anti-CD64	98.47 ± 5.33 [c]	0.135 ± 0.028 [c]	-21.93 ± 0.85 [c]	98.23 ± 8.82
SLN + SPIONs + Anti-CD64	147.17 ± 8.57 [b,c]	0.173 ± 0.030 [b,c]	-12.86 ± 0.76 [b,c]	- - -
SLN + MTX + SPIONs + Anti-CD64	161.13 ± 3.13 [b,c]	0.171 ± 0.023 [b,c]	-14.01 ± 0.80 [b,c]	105.68 ± 4.75

Values shown in mean ± standard deviation (n≥3)
a – Significantly different (p≤0.05), between non-conjugated formulations.
b – Significantly different (p≤0.05), between conjugated formulations.
c – Significantly different (p≤0.05), between after and before functionalization.

5.1.1. Nanoparticle size, Polydispersion Index and Zeta Potential

It has been widely documented that NPs for intravenous applications should present sizes in the range of 100 to 300 nanometers [18, 77, 78]. It has also been verified that particles around 250 nm are more easily incorporated into macrophages [30, 79], which are the primary target cells of this proposed approach. All of the NP formulations presented diameters that were comprised from 100 to 250 nm (Table 2-1), making them suitable for the intended administration route.

Regarding the non-conjugated formulations a significant increase in size can be observed when SPIONs are encapsulated into the SLNs whereas the encapsulation of MTX does seem to influence significantly the size of the NPs. These results suggest that the SPIONs could be altering the structure and/or organization of the lipids in the SLN matrix. Conjugated formulations presented unexpected results, the association of anti-CD64 should increase the NP diameter yet the results showed that the opposite occurred (Table 2-1). Upon a more thorough analysis if the DLS results it was observed that the smaller populations of NPs were more numerous (larger particles diffract more intensity of light [70]). During the functionalization procedure the NP formulations were diluted approximately 400x, during this dilution only the smaller NPs could have been collected leading to a decrease in the particle's overall dimensions that might justify the unexpected results. Considering the size distribution profile, the PdI values, for all of the formulations considered, were below the reference

value of 0.3, which is indicative of mono-dispersed NP populations presenting uniform NP diameters with little agglomeration [70].

Concerning the zeta potential results, all the prepared formulations presented distinct negative values (Table 2-1). The surface charge of SLNs depend on the lipids and the surfactant used, particular cetyl palmimate and Tween 60 SLNs present a negative surface charge that decreases (value in modulus increases) with the percentage of Tween 60 used due to its oxygen-rich head groups. Additionally, stearic acid was also incorporated into the SLN and lead to a decrease in zeta potential values (results obtained during the NP optimization phase) due to the increase of carboxylic groups on the SLN surface, potentially increasing the formulation stability. It has been described that negatively charged particles have reduced cellular uptake, due to electrostatic repulsion between them and the cellular membrane, but also show less cytotoxicity that cationic NPs that can have been proven to be able to disrupt the cellular membrane and consequently cell death [41, 43, 59].

A slight increase (value in modulus decrease) in zeta potential values was seen with the encapsulation of SPIONs into the SLN (Table 2-1). This was not expected since the SPIONs were coated with oleic acid (hydrophobic) and should, for this reason, be located in the core of the NP, having no significant influence in the surface properties. However, the increase of zeta potential after NP functionalization was expected. The antibody conjugation process, previously described, was based on a reaction between the antibody's primary amine and the carboxylic group on the surface charge. This causes to potential reasons for zeta potential reaction: i) the antibody itself presents an overall positive charge that particle's charge to increase even if just slightly [80], and ii) the conjugation reaction causes a shielding around the carboxylic groups that are used to bind the antibody resulting in an increase of the zeta potential.

Although some results are quite as expected they still suggest the proposed formulations are viable and promising candidates for theranostic applications.

5.1.1.1. Nanoparticle formulations stability

In order to assess the stability of developed formulations, NP size, PdI and zeta potential were measured for all of the formulations over the period of one month with three time points (one day, seven days and twenty eight days after NP production), results shown in figure 5-2. It can be seen that over the period of twenty eight days the formulations remain their properties regarding size, PdI and zeta potential allowing to conclude that the developed formulations are stable for at least one month.

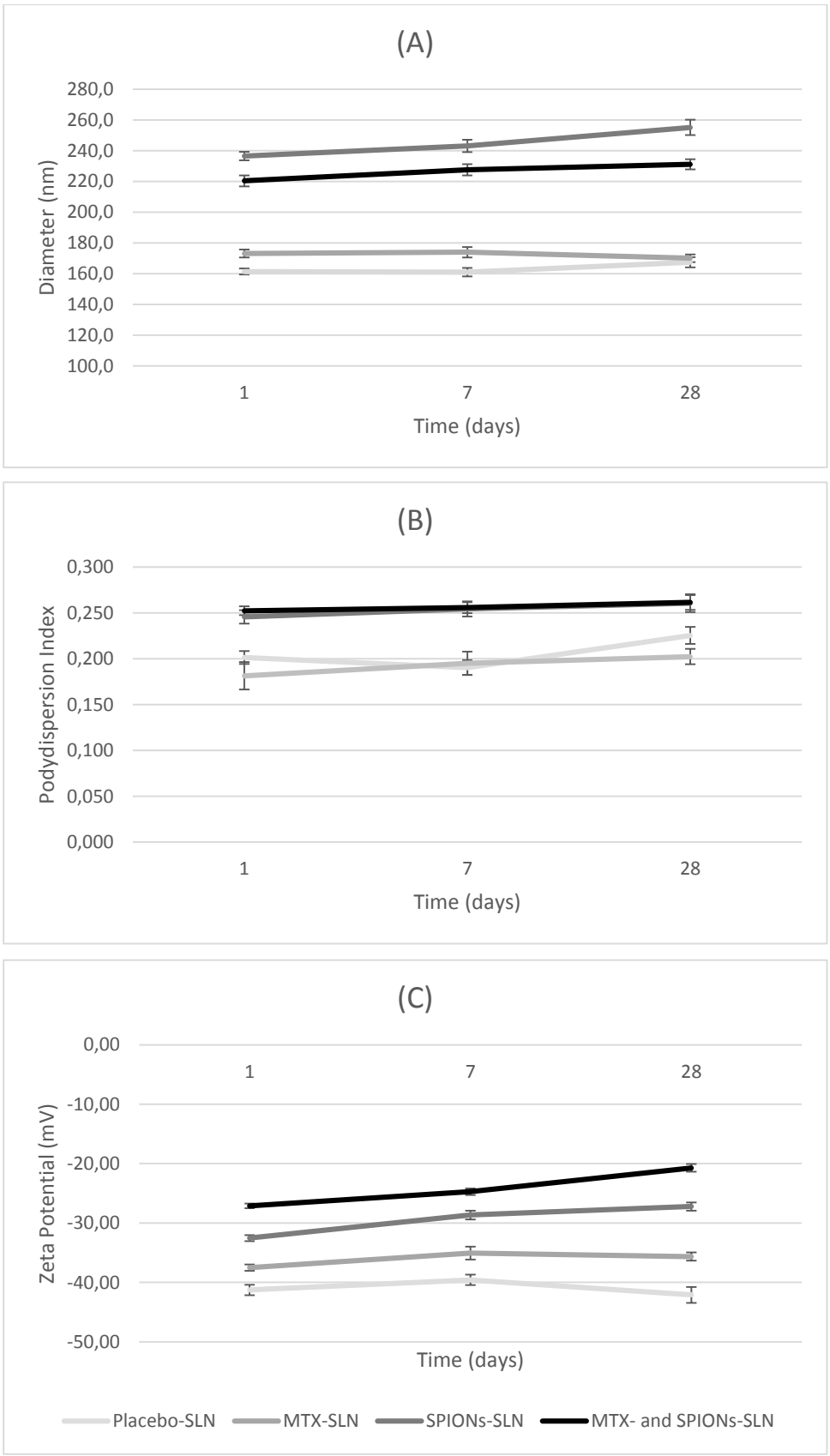

Figure 5-2 – NP properties stability results showing NP diameter (A), PdI (B) and Zeta potential (C). Results shown as mean ± standard deviation (n = 3).

5.1.2. Transmission electron microscopy

TEM photographs (Figure 5-2 and Figure 5-3) were taken to corroborate NP size and poly dispersion as well as access NP morphology and SPION encapsulation. TEM allowed to confirm the sizes and size polydispersions that were previously measured using DLS when considering the placebo and MTX-loaded SLNs (Figure 5-2 A1, A2, B1, B2) and also showed that the encapsulation of MTX didn't influence the NPs shape. The functionalization of the SLNs also didn't seem to alter the shape of the SLNs that maintained their round spherical-shape (Figure 5-2 E1, E2, F1, F2). The same could not be said for the formulations that were encapsulated with SPIONs (Figure 5-2 D1, D2 and Figure 5-3 G1, G2, H1, H2). These formulations showed disfigured NPs that in some case formed agglomerations with undefined morphology.

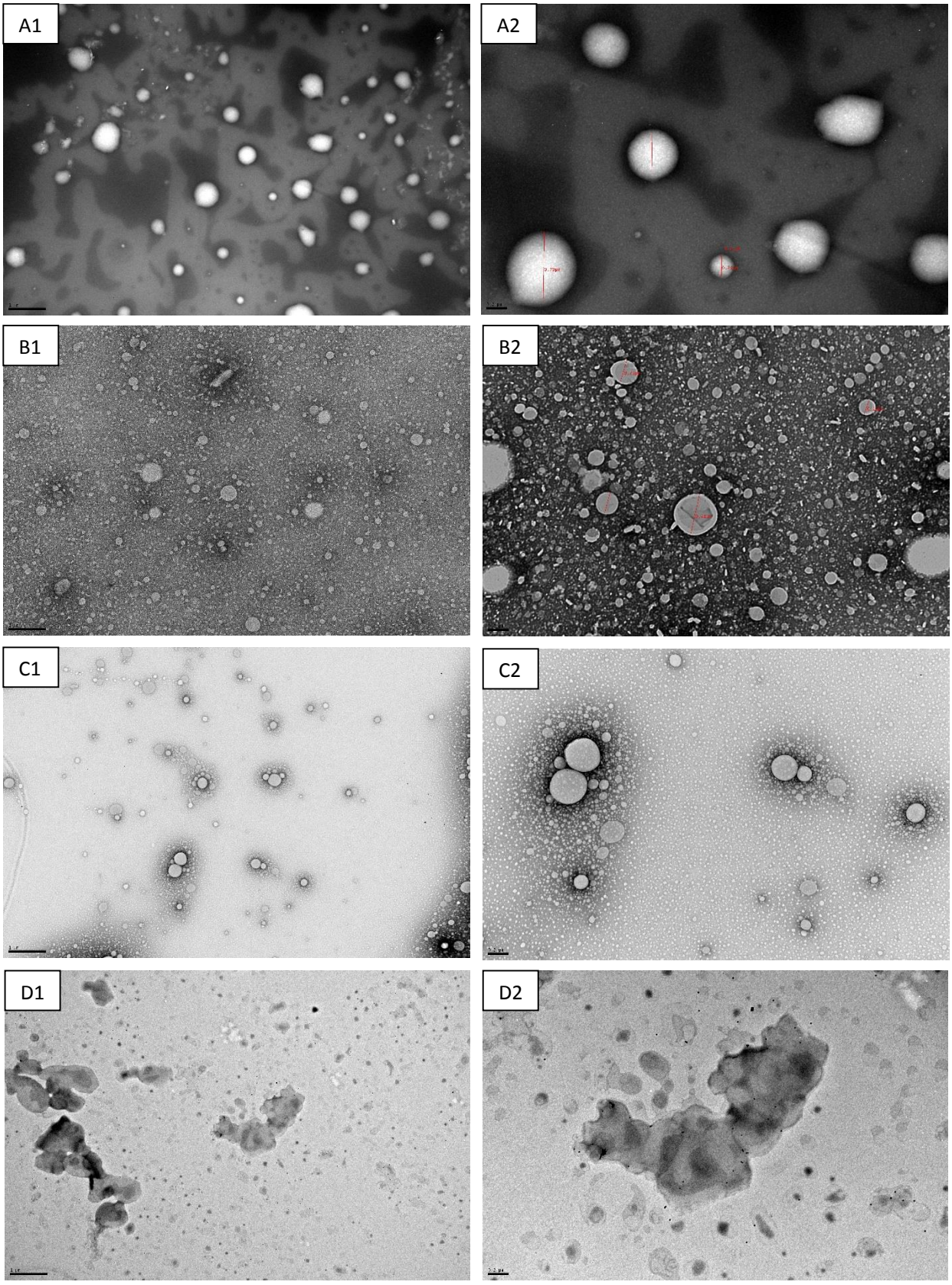

Figure 5-3 – Transmission electron photographs of (A1, A2) cetyl palmitate NPs, (B1, B2) MTX-loaded cetyl palmitate NPs, (C1, C2) SPIONs-loaded cetyl palmitate and (D1, D2) MTX- and SPIONs-loaded cetyl palmitate. (A1, B1, C1, D1) total magnification of 15000x with a scale bar corresponding to 1 µm. (A2, B2, C2, D2) total magnification of 40000x with a scale bar corresponding to 0.2 µm.

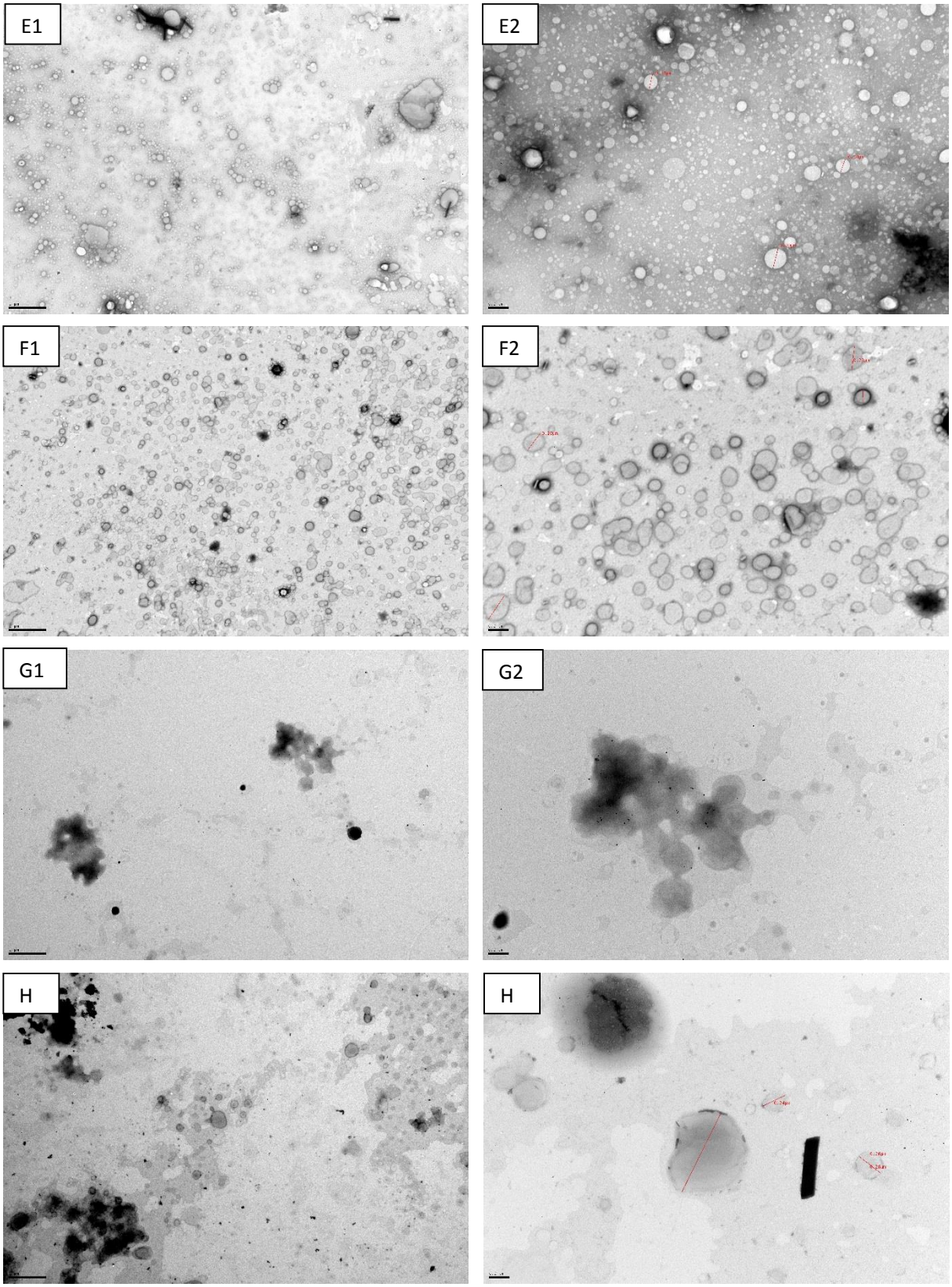

Figure 5-4 - Transmission electron photographs of (E1, E2) anti-CD64 conjugated cetyl palmitate NPs, (F1, F2) anti-CD64 conjugated MTX-loaded cetyl palmitate NPs, (G1, G2) anti-CD64 conjugated SPIONs-loaded cetyl palmitate and (H1, H2) anti-CD64 conjugated MTX- and SPIONs-loaded cetyl palmitate. (E1, F1, G1, H1) total magnification of 15000x with a scale bar corresponding to 1 µm. (E2, F2, G2, H2) total magnification of 40000x with a scale bar corresponding to 0.2 µm.

The photographs taken by TEM (Figure 5-2 D1, D2 and Figure 5-3 G1, G2, H1, H2) were able to verify the encapsulation of the SPIONs inside the SLN matrix, although they were found in the periphery of the matrix instead of in the core and present in fewer number than expected [35]. These unexpected results allow for some conclusions to be taken: i) the agglomerations observed help to explain the increase in size detected in the DLS results and ii) the fact that SPIONs are located in the inner periphery of lipid matrix could explain the increase in zeta potential when SPIONs were encapsulated into SLNs. The SPIONs are coated with oleic acid, making them hydrophobic, and their presence in the periphery of the SLN could cause for a re-organization of lipids on the interface between the lipid and the surfactant leading an increase in zeta potential. This increase en zeta could be sufficient to reduce the formulation overall stability (as explained previously in the correlation between zeta potential and formulation stability) and cause the agglomerations observed in the TEM photographs.

5.1.3. MTX association efficiency

The FT-IR spectrum of MTX-loaded SLNs and placebo SLNs were compared with the spectrum for MTX alone (Figure 5-4). On the MTX spectrum at 1638 cm^{-1} a peak can be observed, this peak corresponds to a carbon-carbon double bond [81]. This bond is characteristic of the drug and is not present on any other compound present on the formulations. This peak, yet faintly, can be seen in the MTX-loaded SLNs but not in the SLNs proving the presence of MTX in the formulation.

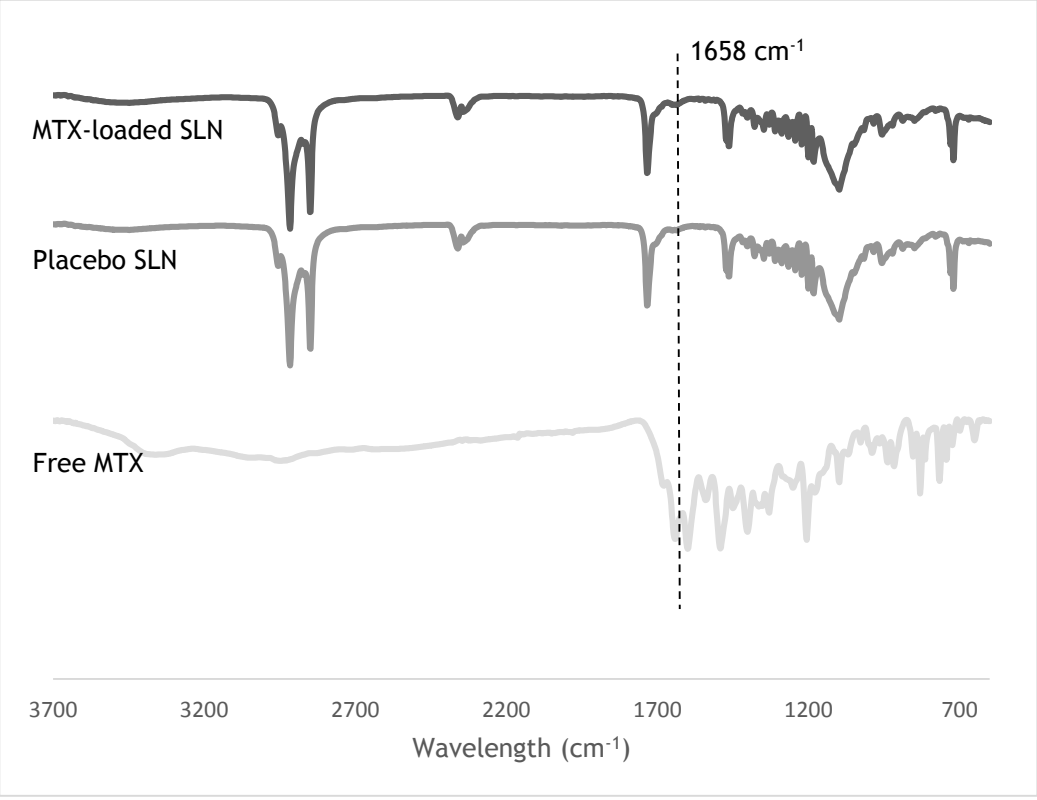

Figure 5-5 – FT-IR spectrum for MTX-loaded SLNs, placebo SLNs and free MTX.

Since the FT-IR is only a qualitative method the encapsulation of MTX was determined by UV/Vis Spectrophotometry. The MTX encapsulation was of 95% and of 105%, for MTX-loaded SLNs and for MTX- and SPIONs-loaded SLNS respectively. Both encapsulation values are similar and close to 100% encapsulation, indicating that the co-encapsulation of MTX and SPIONs is possible and may show promise for future theranostic applications.

5.1.4. Antibody conjugation

The FT-IR spectrum of anti-CD64-conjugated SLNs and placebo SLNs were compared with the spectrum for Anti-CD64 alone (Figure 5-5). On the anti-CD64 spectrum at 1560 cm^{-1} a peak can be observed, this peak corresponds to a nitrogen-hydrogen bond [82]. This bond is characteristic of the drug and is not present on any other compound present on the formulations, since there is no nitrogen. By analyzing the spectrum of the anti-CD64 SLNs it is possible to observe a peak at around 1560 cm^{-1} indicating the presence of a nitrogen-hydrogen bond that, as expected, is not present in the non-conjugated SLNs denoting the presence of the antibody in the SLNs.

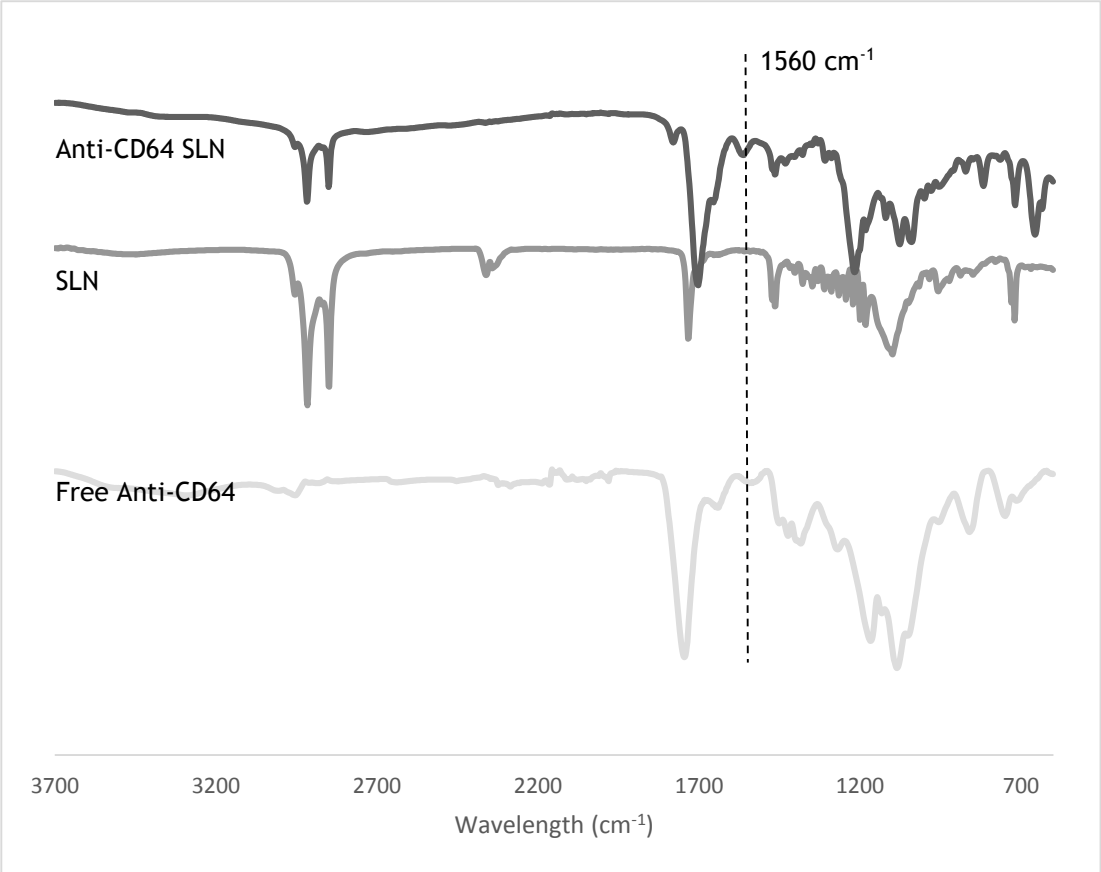

Figure 5-6 FT-IR spectrum for Anti-CD64 conjugated SLNs, non-conjugated SLNs and free anti-CD64.

The quantification of anti-body conjugated was to be performed as previously described, but due to incidents regarding the experimental process has not yet possible to quantify.

5.2. In vitro Assays

5.2.1. Cellular viability and cytotoxicity

In order to assess the effects of the developed NP formulations on cellular viability and overall cytotoxicity, MTT and LDH assays were performed, respectively, on THP-1 cells (differentiated by 24h of incubation with PMA). On both tests, the values obtained for the cells incubated with the NPs controls were used: cells incubated only with culture medium and PBS for the MTT assay and cells treated with Triton X-100 for the LDH assay, as described in the methods sections. A control of free MTX was also included, this control considered the potentially encapsulated MTX, with an association efficiency of 100% (1 mg of MTX per 100 mg of formulation) since MTX is highly hydrophobic at the pH used [83].

Regarding these assays, the expected outcomes were that the placebo-SLN and the SPIONs-loaded SLN formulation would present no cytotoxicity since the components they contain have been shown to be biocompatible [41, 46, 56, 79] and the surfactant was not at high enough concentrations to be toxic [84]. Whereas the formulations that contained MTX (MTX-loaded SLNs and MTX- and SPIONs-loaded SLNs) should influence cellular viability and present cytotoxicity since MTX disrupts aspects of cellular metabolism and therefore decreases the cellular proliferation [9, 85].

The results, however, were not as expected. The MTT assay (Figure 5-6) showed little variation between the cellular viability of cells incubated with NPs of different formulations (comparing among the same concentration). This could be explained considering the reduced amount of MTX added to the formulations that simply could have not been enough to achieve toxic levels. On the other hand only the cells incubated with the highest concentrations of NPs impaired the cellular viability that confirms that the formulations are indeed biocompatible and well accepted by the cells. It is also important to note that the cells incubated with the higher concentrations of free-MTX showed greatly increased viability that was probably due to interferences cause by the large quantities of MTX present in the solution. The LDH assay results (Figure 5-7) corroborated the MTT results regarding the effects of the different formulations and concentrations, showing an increased cytotoxicity in the higher concentrations but no significant variances with different formulations. It is also important to take into account that LDH kit does not measure cytotoxicity directly but in turn measures the amount of cells that die due to cellular lysis [76]. The NPs could present cytotoxic behavior and die in a way that does not cause the cellular membrane to disrupt and, therefore, not being detected by this assay.

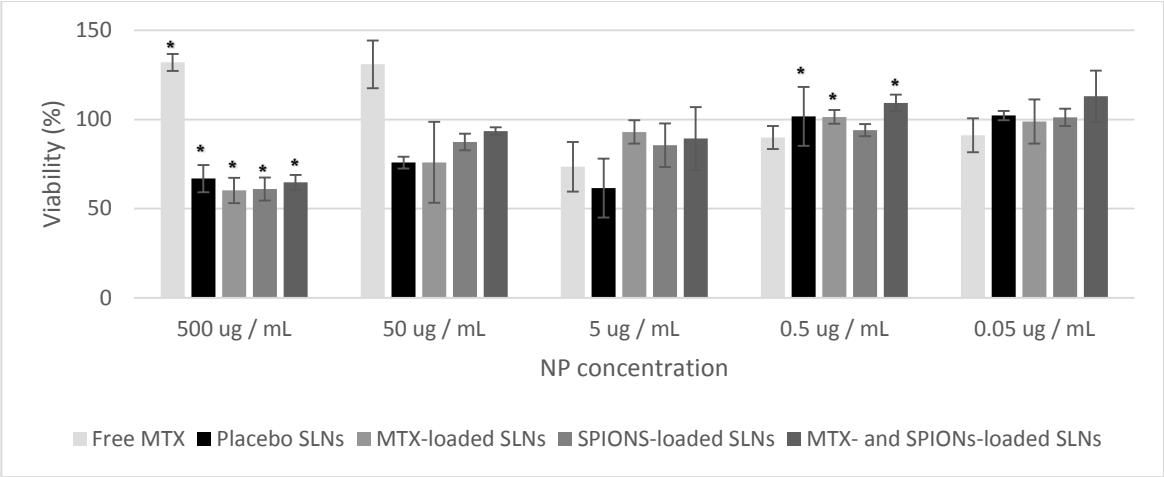

Figure 5-7 – Effect of the developed NP formulations on differentiated THP-1 cells viability as a function of the different NP concentrations (500, 50, 5, 0.5 and 0.05 μg/mL) tested. Values represented as mean ± standard deviation (n≥3; * statistical significant differences assessed with p≤0.05).

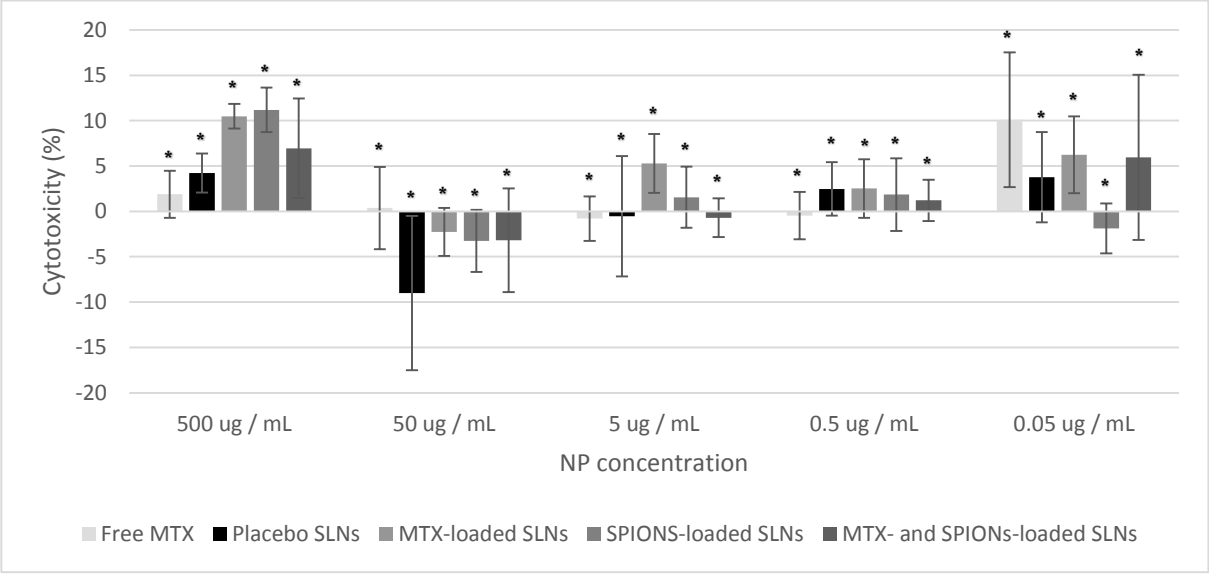

Figure 5-8 – Cytotoxicity of the developed NP formulations on differentiated THP-1 cells as a function of the different NP concentrations (500, 50, 5, 0.5 and 0.05 μg/mL) tested. Values represented as mean ± standard deviation (n≥3; * statistical significant differences assessed with p≤0.05).

- This Page was intentionally left blank -

Conclusions

The use of SLN for simultaneous drug delivery and in vivo imaging is an interesting approach for safe theranostic applications considering their biocompatibility and biodegradability, especially with the new possibilities of multifunctionalization brought by nanomedicine. In this work, an innovative attempt to achieve a combined therapy and imaging of RA was proposed, by co-encapsulating MTX and SPIONs inside cetyl palmitate and stearic acid SLNs. These SLNs were further functionalized with anti-CD64, an antibody that specifically binds to a cell surface receptor that is over expressed in RA infected macrophages.

The proposed NP formulations presented interested and promising results for future theranostics of RA, regarding both physicochemical properties of the NPs as well interaction with the cell line THP-1 differentiated cells.

Concerning the NP characterization, all the formulations presented dimensions comprised between the ranges of 100 nm to 250 nm with PdI values that indicate a monodispersed size profile, making them potential and promising candidates for intravenous administration as proposed. These results were confirmed, to some extent, by TEM that showed spherical morphology for most of the formulations, while also revealing small deformations of the NPs containing SPIONs that help to explain some of the results obtained for these formulations in terms of size and zeta potential.

The zeta potential values for all the formulations were comprise between -12 and -40 mV, as a result of the incorporation of stearic acid that integrated the surface of the SLNs leaving it's carboxylic group outwards and exposed. This addition to the formulation not only increased the functional groups available for future functionalization purposes but also helped to stabilize the formulations. The addition of MTX did not alter the zeta values very significantly, whereas the addition of SPIONs caused the values to increase slightly. This was explained by the previously mentioned TEM results, which showed a preferential accumulation of SPIONs in the periphery of the NPs. The SPIONs were coated with oleic acid that probably caused a re-organization of the lipids in periphery that could explain the difference in the zeta potential.

It was also proven that all of the NP formulations are stable up to one month, with little alterations in NP size, PdI and zeta potential over this period of time.

The encapsulation of both MTX and SPIONs into the formulations was suspected immediately after NP production due to the alterations observed in the colors of those same formulations. The association of MTX to the formulations was verified by FT-IR spectroscopy that indicated specific peaks that were characteristic of the MTX but not the other components present. The association of MTX was also quantified by UV/Vis spectrophotometry, and efficiencies of 98% and 105% for the MTX-loaded SLNs and for the MTX- and SPIONs-loaded SLNs. The encapsulation of SPIONs was proven by

TEM, as small very electro dense dots rounding 10 nm in diameter were observed within the SLN matrix.

The successful antibody conjugation was hinted in the zeta potential values, which increased (decreased in modulus) in all the formulations after antibody conjugation. This hypothesis was verified using FT-IR spectroscopy that enable the verification of peak specific to the antibody and not present in the SLN components.

Finally the *in vitro* assays showed that the NPs presented low toxicity after 24h of incubation to THP-1 cell line, with exception for the highest concentrations. Proving that the proposed formulations were indeed safe for future theranostic applications.

In conclusion, the results proved that the proposed formulations are very promising for the future of RA treatment and diagnostic/monitoring, by providing a safe and targeted delivery of therapeutic agents and simultaneously allowing *in vivo* imaging. There is, however, still much to be done and more comprehensive and detailed studies should be performed in order for approaches such as this one to leave the lab and move to the clinic, but the pavement is being laid for such a time.

Future work

In order to further characterize the NP formulations, the efficiency of antibody-conjugation should be assessed as well as the effects of antibody-conjugated NP on the viability and cytotoxicity in *in vitro* assays. Studies to optimize the amount of MTX and SPIONs encapsulation in the formulations should also be performed in order to maximize the therapeutic effect and imaging capability. Similar studies should also be performed to optimize the antibody ratio. Studies to determine the crystallization degree of encapsulated-MTX would also be recommended, since this degree will influence drug release.

Considering SLN production method, a purification procedure should also be added in order to allow the removal of production/conjugation excesses. A potential procedure would be ultra-centrifugation of the formulations, such a process would also have to be optimize to ensure proper separation between the NPs and the suspension medium.

Regarding the NP characterization, studies using SPIONs non-coated with oleic acid could be performed, in order to assess if they could be encapsulated with altering the stability of the SLNs (as explained in the TEM results).

Concerning the *in vitro* assays, cellular uptake assays should be performed to determine whether or not the NPs are actually penetrating the cellular membrane and what is the internalization mechanism responsible for this.

Looking a bit further down the road, perhaps a secondary functionalization with PEG-chains in order to make the particle less recognizable to the immune system increasing its potential effectiveness as a theranostic agent. Such a coating could also alter the antibody conjugation tested in the assay, by linking the antibody to the end of the PEG-chain with all the added benefits.

- This Page was intentionally left blank -

References

1. Seeley, R.R., T.D. Stephens, and P. Tate, Anatomy & Physiology. 8th ed. 2008: McGraw-Hill.

2. Ellis, H., S. Standring, and H.D. Gray, Gray's anatomy: the anatomical basis of clinical practice. 38th ed. 2005: Churchill Livingstone.

3. Smith, A.M., L. Fleming, U. Wudebwe, J. Bowen, and L.M. Grover, Development of a synovial fluid analogue with bio-relevant rheology for wear testing of orthopaedic implants. Journal of the Mechanical Behavior of Biomedical Materials, 2013.

4. Lee, D. and M. Weinblatt, Rheumatoid arthritis. The Lancet, 2001. 358(9285): p. 903-911.

5. Majithia, V. and S.A. Geraci, Rheumatoid arthritis: diagnosis and management. Am J Med, 2007. 120(11): p. 936-9.

6. Scott, D.L., F. Wolfe, and T.J.W. Huizinga, Rheumatoid Arthirtis. Lancet, 2010. 376.

7. Choy, E.H., A.F. Kavanaugh, and S.A. Jones, The problem of choice: current biologic agents and future prospects in RA. Nat Rev Rheumatol, 2013. 9(3): p. 154-63.

8. Maciejewska Rodrigues, H., A. Jungel, R.E. Gay, and S. Gay, Innate immunity, epigenetics and autoimmunity in rheumatoid arthritis. Mol Immunol, 2009. 47(1): p. 12-8.

9. Cutolo, M., A. Sulli, and C. Pizzorni, Anti-inflammatory mechanisms of methotrexate in rheumatoid arthritis. Ann Rheum Dis, 2001.

10. Taouli, B., S. Zaim, C.G. Peterfy, J.A. Lynch, A. Stork, A. Guermazi, B. Fan, K.H. Fye, and H.K. Genant, Rheumatoid Arthritis of the Hand and Wrist: Comparison of Three Imaging Techniques. AJR Am J Roentgenol, 2003.

11. Boutry, N., M. Morel, R.M. Flipo, X. Demondion, and A. Cotten, Early rheumatoid arthritis: a review of MRI and sonographic findings. AJR Am J Roentgenol, 2007. 189(6): p. 1502-9.

12. Narváez, J.A., J. Narváez, E. De Lama, and M. De Albert, MR Imaging of Early Rheumatoid Arthritis. RadioGraphics, 2010.

13. Smolen, J.S., D. Aletaha, M. Koeller, M.H. Weisman, and P. Emery, New therapies for treatment of rheumatoid arthritis. The Lancet, 2007. 370(9602): p. 1861-1874.

14. Smolen, J.S., D. Aletaha, J.W. Bijlsma, F.C. Breedveld, D. Boumpas, G. Burmester, B. Combe, M. Cutolo, M. de Wit, M. Dougados, P. Emery, A. Gibofsky, J.J. Gomez-Reino, B. Haraoui, J. Kalden, E.C. Keystone, T.K. Kvien, I. McInnes, E. Martin-Mola, C. Montecucco, M. Schoels, D. van der Heijde, and T.T.E. Committee, Treating rheumatoid arthritis to target: recommendations of an international task force. Ann Rheum Dis, 2010. 69(4): p. 631-7.

15. Chakravarty, S.D., P.I. Poulikakos, L.B. Ivashkiv, J.E. Salmon, and G.D. Kalliolias, Kinase inhibitors: a new tool for the treatment of rheumatoid arthritis. Clin Immunol, 2013. 148(1): p. 66-78.

16. de la Rica, L., J.M. Urquiza, D. Gomez-Cabrero, A.B. Islam, N. Lopez-Bigas, J. Tegner, R.E. Toes, and E. Ballestar, Identification of novel markers in rheumatoid arthritis through integrated analysis of DNA methylation and microRNA expression. J Autoimmun, 2013. 41: p. 6-16.

17. Lembo, D. and R. Cavalli, Nanoparticulate delivery systems for antiviral drugs. Antivir Chem Chemother, 2010. 21(2): p. 53-70.

18. Moghimi, S.M., A.C. Hunter, and J.C. Murray, Nanomedicine: current status and future prospects. FASEB J, 2005. 19(3): p. 311-30.

19. Ferrari, M., Cancer nanotechnology: opportunities and challenges. Nat Rev Cancer, 2005. 5(3): p. 161-71.

20. Zhang, L., D. Pornpattananangkul, C.M.J. Hu, and H.C. M., Development of Nanoparticles for Antimicrobial Drug Delivery. Current Medicinal Chemistry, 2010.

21. Bamrungsap, S., Z. Zhao, T. Chen, L. Wang, C. Li, T. Fu, and W. Tan, Nanotechnology in Therapeutics. Nanomedicine, 2012.

22. Sehgal, R., Nanotechnology and Its Applications in Drug Delivery: A Review. International Journal of Medicine and Molecular Medicine, 2013.

23. Mashaghi, S., T. Jadidi, G. Koenderink, and A. Mashaghi, Lipid nanotechnology. Int J Mol Sci, 2013. 14(2): p. 4242-82.

24. Couvreur, P., Nanoparticles in drug delivery: past, present and future. Adv Drug Deliv Rev, 2013. 65(1): p. 21-3.

25. Iqbal, M.A., S. Md, J.K. Sahni, S. Baboota, S. Dang, and J. Ali, Nanostructured lipid carriers system: recent advances in drug delivery. J Drug Target, 2012. 20(10): p. 813-30.

26. Gref, R., P. Quellec, A. Sanchez, P. Calvo, E. Dellacherie, and M.J. Alonso, Development and characterization of CyA-loaded poly(lactic acid)±poly(ethylene glycol)PEG micro- and nanoparticles. Comparison with conventional PLA particulate carriers. Eur J Pharm Biopharm, 2001.

27. Lu, A.H., E.L. Salabas, and F. Schuth, Magnetic nanoparticles: synthesis, protection, functionalization, and application. Angew Chem Int Ed Engl, 2007. 46(8): p. 1222-44.

28. Goutayer, M., S. Dufort, V. Josserand, A. Royere, E. Heinrich, F. Vinet, J. Bibette, J.L. Coll, and I. Texier, Tumor targeting of functionalized lipid nanoparticles: assessment by in vivo fluorescence imaging. Eur J Pharm Biopharm, 2010. 75(2): p. 137-47.

29. Essa, S., J.M. Rabanel, and P. Hildgen, Effect of polyethylene glycol (PEG) chain organization on the physicochemical properties of poly(D, L-lactide) (PLA) based nanoparticles. Eur J Pharm Biopharm, 2010. 75(2): p. 96-106.

30. Martins, S., I. Tho, I. Reimold, G. Fricker, E. Souto, D. Ferreira, and M. Brandl, Brain delivery of camptothecin by means of solid lipid nanoparticles: formulation design, in vitro and in vivo studies. Int J Pharm, 2012. 439(1-2): p. 49-62.

31. Martins, S.M., B. Sarmento, C. Nunes, M. Lucio, S. Reis, and D.C. Ferreira, Brain targeting effect of camptothecin-loaded solid lipid nanoparticles in rat after intravenous administration. Eur J Pharm Biopharm, 2013. 85(3): p. 488-502.

32. Coco, R., L. Plapied, V. Pourcelle, C. Jerome, D.J. Brayden, Y.J. Schneider, and V. Preat, Drug delivery to inflamed colon by nanoparticles: comparison of different strategies. Int J Pharm, 2013. 440(1): p. 3-12.

33. Sapsford, K.E., W.R. Algar, L. Berti, K.B. Gemmill, B.J. Casey, E. Oh, M.H. Stewart, and I.L. Medintz, Functionalizing nanoparticles with biological molecules: developing chemistries that facilitate nanotechnology. Chem Rev, 2013. 113(3): p. 1904-2074.

34. Pan, H., J.W. Myerson, L. Hu, J.N. Marsh, K. Hou, M.J. Scott, J.S. Allen, G. Hu, S. San Roman, G.M. Lanza, R.D. Schreiber, P.H. Schlesinger, and S.A. Wickline, Programmable nanoparticle functionalization for in vivo targeting. FASEB J, 2013. 27(1): p. 255-64.

35. Moura, C.d.C., Development of Multifunctional Nanoparticles for Targeted Therapy and Imaging of Rheumatoid Arthritis, in Faculdade de Engenharia. 2013, Universidade do Porto. p. 60.

36. Machado, M., Transdermal delivery of pH responsive liposomes containing indomethacin for the treatment of Rheumatoid Arthritis, in Faculdade de Engenharia. 2013, Universidade do Porto. p. 84.

37. Venishetty, V.K., R. Chede, R. Komuravelli, L. Adepu, R. Sistla, and P.V. Diwan, Design and evaluation of polymer coated carvedilol loaded solid lipid nanoparticles to improve the oral bioavailability: a novel strategy to avoid intraduodenal administration. Colloids Surf B Biointerfaces, 2012. 95: p. 1-9.

38. Patil, S.M. and H.P. Hemant P Joshi, Lipid shell modified with combination oflipid and phospholipids in solid lipid nanoparticles for engineered specificity of paclitaxel in tumor bearing mice. International Journal of Drug Delivery, 2013.

39. Weber, S., A. Zimmer, and J. Pardeike, Solid Lipid Nanoparticles (SLN) and Nanostructured Lipid Carriers (NLC) for pulmonary application: A review of the state of the art. Eur J Pharm Biopharm, 2013.

40. Muller, R.H., K. Mader, and S. Gohla, Solid lipid nanoparticles (SLN) for controlled drug delivery - a review of the state of the art. Eur J Pharm Biopharm, 2000.

41. Ekambaram, P., A.A.H. Satahali, and K. Priyanka, Solid Lipid Nanoparticles: Review. Sci. Revs. Chem. Commun., 2012.

42. Muhlen, A., C. Schwarz, and W. Mehnert, Solid lipid nanoparticles (SLN) for controlled drug delivery – Drug release and release mechanism. Eur J Pharm Biopharm, 1998.

43. Weyhers, H., S. Ehlers, H. Hahn, E.B. Souto, and R.H. Muller, Solid Lipid Nanoparticles (SLN) – Effects of lipid composition on in vitro degradation and in vivo toxicity. Pharmazie, 2006.

44. Jayagopal, A., E.M. Sussman, and V.P. Shastri, Functionalized Solid Lipid Nanoparticles for Transendothelial Delivery. IEEE, 2008.

45. Alukda, D., T. Sturgis, and B.B. Youan, Formulation of tenofovir-loaded functionalized solid lipid nanoparticles intended for HIV prevention. J Pharm Sci, 2011. 100(8): p. 3345-56.

46. Mehnert, W. and K. Mader, Solid lipid nanoparticles: Production, characterization and applications. Advanced Drug Delivery Reviews, 2001.

47. Hou, D., C. Xie, K. Huang, and C. Zhu, The production and characteristics of solid lipid nanoparticles (SLNs). Biomaterials, 2003. 24(10): p. 1781-1785.

48. Westesen, K., H. Bunjes, and M.H.J. Koch, Physicochemical characterization of lipid nanoparticles and evaluation of their drug loading capacity and sustained release potential. Journal of Controlled Release, 1997.

49. Torchilin, V.P., Recent advances with liposomes as pharmaceutical carriers. Nat Rev Drug Discov, 2005. 4(2): p. 145-60.

50. Bitounis, D., R. Fanciullino, A. Iliadis, and J. Ciccolini, Optimizing Druggability through Liposomal Formulations: New Approaches to an Old Concept. ISRN Pharm, 2012. 2012: p. 738432.

51. Bochot, A. and E. Fattal, Liposomes for intravitreal drug delivery: a state of the art. J Control Release, 2012. 161(2): p. 628-34.

52. Kung, C., A possible unifying principle for mechanosensation. Nature, 2005. 436(7051): p. 647-54.

53. Duangjit, S., B. Pamornpathomkul, P. Opanasopit, T. Rojanarata, Y. Obata, K. Takayama, and T. Ngawhirunpat, Role of the charge, carbon chain length, and content of surfactant on the skin penetration of meloxicam-loaded liposomes. Int J Nanomedicine, 2014. 9: p. 2005-17.

54. Dai, W., F. Yang, L. Ma, Y. Fan, B. He, Q. He, X. Wang, H. Zhang, and Q. Zhang, Combined mTOR inhibitor rapamycin and doxorubicin-loaded cyclic octapeptide modified liposomes for targeting integrin alpha3 in triple-negative breast cancer. Biomaterials, 2014. 35(20): p. 5347-58.

55. Ninomiya, K., S. Kawabata, H. Tashita, and N. Shimizu, Ultrasound-mediated drug delivery using liposomes modified with a thermosensitive polymer. Ultrason Sonochem, 2014. 21(1): p. 310-6.

56. Almeida, A.J., S. Runge, and R.H. Muller, Peptide-loaded solid lipid nanoparticles (SLN): influence of production parameters. International Journal of Pharmaceutics, 1997.

57. Tabatt, K., C. Kneuer, M. Sameti, C. Olbrich, R.H. Muller, C.M. Lehr, and U. Bakowsky, Transfection with different colloidal systems: comparison of solid lipid nanoparticles and liposomes. J Control Release, 2004. 97(2): p. 321-32.

58. Jores, K., W. Mehnert, M. Drechsler, H. Bunjes, C. Johann, and K. Mader, Investigations on the structure of solid lipid nanoparticles (SLN) and oil-loaded solid lipid nanoparticles by photon correlation spectroscopy, field-flow fractionation and transmission electron microscopy. J Control Release, 2004. 95(2): p. 217-27.

59. Üner, M. and G. Yener, Importance of solid lipid nanoparticles (SLN) in various administration routes and future perspective. International Journal of Nanomedicine, 2007. 2(3).

60. Hsu, M.H. and Y.C. Su, Iron-oxide embedded solid lipid nanoparticles for magnetically controlled heating and drug delivery. Biomed Microdevices, 2008. 10(6): p. 785-93.

61. Zhang, Z.H., Y.L. Zhang, J.P. Zhou, and H.X. Lv, Solid lipid nanoparticles modified with stearic acid-octaarginine for oral administration of insulin. Int J Nanomedicine, 2012. 7: p. 3333-9.

62. Shastri, V., E. Sussman, and A. Jayagopal, Functionalized solid lipid nanoparticles and methods of making and using same. 2006, Google Patents: US.

63. Zhang, W., J. Liu, Q. Zhang, X. Li, S. Yu, X. Yang, J. Kong, and W. Pan, Enhanced cellular uptake and anti-proliferating effect of chitosan hydrochlorides modified genistein loaded NLC on human lens epithelial cells. Int J Pharm, 2014. 471(1-2): p. 118-26.

64. Jain, K., S. Sood, and K. Gowthamarajan, Optimization of artemether-loaded NLC for intranasal delivery using central composite design. Drug Deliv, 2014.

65. Mussi, S.V., R. Sawant, F. Perche, M.C. Oliveira, R.B. Azevedo, L.A. Ferreira, and V.P. Torchilin, Novel Nanostructured Lipid Carrier Co-Loaded with Doxorubicin and Docosahexaenoic Acid Demonstrates Enhanced in Vitro Activity and Overcomes Drug Resistance in MCF-7/Adr Cells. Pharm Res, 2014.

66. Aubin-Tam, M.E. and K. Hamad-Schifferli, Structure and function of nanoparticle-protein conjugates. Biomed Mater, 2008. 3(3): p. 034001.

67. Sperling, R.A. and W.J. Parak, Surface modification, functionalization and bioconjugation of colloidal inorganic nanoparticles. Philos Trans A Math Phys Eng Sci, 2010. 368(1915): p. 1333-83.

68. Sussman, E.M., A. Jayagopal, F.R. Haselton, and V.P. Shastri, Engineering of Solid Lipid Nanoparticles for Biomedical Applications, in New Delivery Systems for Controlled Drug Release from Naturally Occurring Materials, N. Parris, et al., Editors. 2008, American Chemical Society. p. 139-152.

69. Curnow, R.T., Clinical experience with CD64-directed immunotherapy. An overview. Cancer Immunology Immunotherapy, 1997.

70. Block, I.A., Particle sizing by 3D cross-correlation DLS in highly scattering samples. 2010, LS Instruments.

71. Gimsa, J., P. Eppmann, and B. Prujger, Introducing Phase Analysis Light Scattering for Dielectric Characterization: Measurement of Traveling-Wave Pumpin. Biophysical Journal, 1997.

72. (c) Thermo Nicolet Corporation: Introduction to Fourier Transform Infrared Specroscopy. 2001.

73. Instructions: Coomassie PlusTM (Bradford) Assay Kit. Thermo Scientific.

74. ATCC (R) THP-1 (ATCC (R) TIB-202TM).

75. MTT Cell Proliferation Assay Instruction Guide. 2011, ATCC (R).

76. LDH Cytotoxicity Detection Kit - Product Manual. Takara Bio Inc.

77. Williams, J., R. Lansdown, R. Sweitzer, M. Romanowski, R. LaBell, R. Ramaswami, and E. Unger, Nanoparticle drug delivery system for intravenous delivery of topoisomerase inhibitors. Journal of Controlled Release, 2003. 91(1-2): p. 167-172.

78. Yang, S.C.L., L. F., Y. Cai, J.B. Zhu, B.W. Liang, and C.Z. Yang, Body distribution in mice of intravenously injected camptothecin solid lipid nanoparticles and targeting effect on brain. Journal of Controlled Release, 1999.

79. Scholer, N., H. Hahn, R.H. Muller, and O. Liesenfeld, Effect of lipid matrix and size of solid lipid nanoparticles (SLN) on the viability and cytokine production of macrophages. International Journal of Pharmaceutics, 2002.

80. Raamsdonk, M.M., H. C., J.J. Soet, H.J. Busscher, and J. Graaff, Effect of Polyclonal and Monoclonal antibodies on Surface properties of Streptococcus Sobrinus. Infection and Immunity, 1995.

81. Sibeko, B., Y.E. Choonara, L.C. du Toit, G. Modi, D. Naidoo, R.A. Khan, P. Kumar, V.M. Ndesendo, S.E. Iyuke, and V. Pillay, Composite polylactic-methacrylic Acid copolymer nanoparticles for the delivery of methotrexate. J Drug Deliv, 2012. 2012: p. 579629.

82. Shukla, N., C. Liu, P.M. Jones, and D. Weller, FTIR study of surfactant bonding to FePt nanoparticles. Journal of Magnetism and Magnetic Materials, 2003. 266(1-2): p. 178-184.

83. Houngbossa, K., J. Guenzet, and M. Bourin, Effets de la température et du pH sur la cinétique de dissolution du méthotrexato en milieu aqueux. Annales Pharmaceutiques Françaises, 1996.

84. Arechabala, B., C. Coiffard, P. Rivalland, L.J.M. Coiffard, and Y. Roeck-Holtzhauer, Comparison of Cytotoxicity of Various Surfactants Tested on Normal Human Fibroblast Cultures using the Neutral Red Test, MTT Assay and LDH Release. OURNAL OF APPLIED TOXICOLOGY, 1999.

85. Widemann, B.C. and P.C. Adamson, Understanding and Managing Methotrexate Nephrotoxicity. The Oncologist, 2006.